Acta Crystallographica Section D
Biological Crystallography
ISSN 1399-0047

Na^+/K^+ exchange switches the catalytic apparatus of potassium-dependent plant L-asparaginase

Magdalena Bejger,[a] Barbara Imiolczyk,[a] Damien Clavel,[b] Miroslaw Gilski,[a,b] Agnieszka Pajak,[c] Frédéric Marsolais[c] and Mariusz Jaskolski[a,b]*

[a]Center for Biocrystallographic Research, Institute of Bioorganic Chemistry, Polish Academy of Sciences, Poznan, Poland, [b]Department of Crystallography, Faculty of Chemistry, A. Mickiewicz University, Poznan, Poland, and [c]Agriculture and Agri-Food Canada, London, Ontario, Canada

Correspondence e-mail: mariuszj@amu.edu.pl

Received 17 March 2014
Accepted 16 April 2014

PDB references: PvAspG1–K/Na, 4pv2; PvAspG1–K, 4pu6; PvAspG1–Na, 4pv3

Plant-type L-asparaginases, which are a subclass of the Ntn-hydrolase family, are divided into potassium-dependent and potassium-independent enzymes with different substrate preferences. While the potassium-independent enzymes have already been well characterized, there are no structural data for any of the members of the potassium-dependent group to illuminate the intriguing dependence of their catalytic mechanism on alkali-metal cations. Here, three crystal structures of a potassium-dependent plant-type L-asparaginase from *Phaseolus vulgaris* (PvAspG1) differing in the type of associated alkali metal ions (K^+, Na^+ or both) are presented and the structural consequences of the different ions are correlated with the enzyme activity. As in all plant-type L-asparaginases, immature PvAspG1 is a homodimer of two protein chains, which both undergo autocatalytic cleavage to α and β subunits, thus creating the mature heterotetramer or dimer of heterodimers $(\alpha\beta)_2$. The $\alpha\beta$ subunits of PvAspG1 are folded similarly to the potassium-independent enzymes, with a sandwich of two β-sheets flanked on each side by a layer of helices. In addition to the 'sodium loop' (here referred to as the 'stabilization loop') known from potassium-independent plant-type asparaginases, the potassium-dependent PvAspG1 enzyme contains another alkali metal-binding loop (the 'activation loop') in subunit α (residues Val111–Ser118). The active site of PvAspG1 is located between these two metal-binding loops and in the immediate neighbourhood of three residues, His117, Arg224 and Glu250, acting as a catalytic switch, which is a novel feature that is identified in plant-type L-asparaginases for the first time. A comparison of the three PvAspG1 structures demonstrates how the metal ion bound in the activation loop influences its conformation, setting the catalytic switch to ON (when K^+ is coordinated) or OFF (when Na^+ is coordinated) to respectively allow or prevent anchoring of the reaction substrate/product in the active site. Moreover, it is proposed that Ser118, the last residue of the activation loop, is involved in the potassium-dependence mechanism. The PvAspG1 structures are discussed in comparison with those of potassium-independent L-asparaginases (LlA, EcAIII and hASNase3) and those of other Ntn-hydrolases (AGA and Tas1), as well as in the light of non-crystallographic studies.

1. Introduction

All enzymes that belong to the Ntn-hydrolase family have an N-terminal nucleophilic (Ntn) residue (Thr, Ser or Cys) that is liberated in an obligatory autoproteolytic activation step from a nonfunctional precursor (Brannigan *et al.*, 1995). This family includes such functionally diverse enzymes as taspase 1 (Tas1; Khan *et al.*, 2005), aspartylglucosaminidases (AGAs; Guo

© 2014 International Union of Crystallography

et al., 1998; Oinonen *et al.*, 1995), plant-type L-asparaginases/isoaspartyl aminopeptidases (Borek & Jaskólski, 2001; Michalska & Jaskolski, 2006) and some other proteins. All of these enzymes are amidohydrolases that process L-asparagine/L-aspartate-derived substrates and they all use threonine as the nucleophilic residue. Moreover, they all share common structural features. Specifically, in the mature form they are folded as heterotetramers or dimers of $\alpha\beta$ heterodimers. The $\alpha\beta$ unit is produced in the autoproteolytic event and has a characteristic $\alpha\beta\beta\alpha$ fold, in which a sandwich of largely antiparallel β-sheets is flanked on both sides by layers of α-helices. The relatively high level of sequence similarity between Tas1, aspartylglucosaminidases and plant-type L-asparaginases (~60%) is consistent with their structural similarity (r.m.s.d. of ~1.9 Å for C^{α} superpositions).

Plant-type L-asparaginases can be further subdivided into potassium-dependent (K-dependent) and potassium-independent (K-independent) enzymes (Sodek *et al.*, 1980), although the two subgroups share a relatively high sequence similarity (~70%). The L-asparaginase activity of the K-independent enzymes is insensitive to the presence of metal cations in the environment. In contrast, the enzymatic activity of the K-dependent proteins is modulated according to the presence of monovalent metal cations. For example, Bruneau *et al.* (2006) showed that the L-asparaginase activity of the K-dependent enzyme from *Arabidopsis thaliana* is highest in the presence of K^+ cations but decreases according to the pattern $Na^+ > Rb^+$ when other alkali metals are used. A similar reactivity sequence, $K^+ > Rb^+ = Na^+ > Cs^+ = Li^+$, was found for the enzyme from *Lotus japonicus* (Credali *et al.*, 2011). However, to date the molecular basis of the potassium dependence has remained unexplained and there is no experimental structure of any plant-type potassium-dependent L-asparaginase. Crystal structures of potassium-independent enzymes have, on the other hand, been determined for *Lupinus luteus* L-asparaginase (LlA; PDB entry 2gez; Michalska *et al.*, 2006) and for two homologous proteins: EcAIII from *Escherichia coli* (PDB entries 1jn9, 1k2x, 1t3m, 2zal, 2zak and 3c17; Borek & Jaskólski, 2000; Borek, 2001; Prahl *et al.*, 2004; Michalska *et al.*, 2005; Michalska, Borek *et al.*, 2008; Michalska, Hernández-Santoyo *et al.*, 2008) and the human asparaginase-like protein hASNase3 (PDB entries 4gdt, 4gdu, 4gdv, 4gdw, 4hlo and 4hlp; Nomme *et al.*, 2012; Su *et al.*, 2013).

Recently, there has been increased interest in engineering hASNase3 for use as a therapeutic agent for the systemic depletion of serum L-asparagine in the treatment of acute lymphoblastic leukaemia (Li *et al.*, 2012; Karamitros & Konrad, 2014). This enzymatic antileukaemic treatment is normally only effective with enzymes having high affinity for L-asparagine (Verma *et al.*, 2007), such as the periplasmic isoenzyme from *E. coli* (EcAII; K_m = 11.5 μM; Ho *et al.*, 1970), which was the first bacterial-type L-asparaginase to have its structure determined (Swain *et al.*, 1993). The K_m values for L-asparagine of typical plant-type L-asparaginases are >100-fold higher than for bacterial-type enzymes, and are in the range 1–30 mM depending on the source organism, the potassium dependence of the enzyme and the ions present in the activity tests. The bacterial-type and plant-type enzymes belong to structurally distinct groups (Borek & Jaskólski, 2001) and their catalytic mechanisms are also different (Michalska & Jaskolski, 2006). Moreover, the plant-type enzymes, besides L-asparaginase activity, have a unique additional isoaspartyl aminopeptidase activity.

The L-asparaginase activity releases ammonia from L-asparagine, which is the most significant metabolite for the storage and transport of nitrogen in plants. This activity provides nitrogen for protein biosynthesis and is particularly important in fast-developing tissues (*e.g.* shoots) and during the formation of seeds, when storage proteins are synthesized. The isoaspartylpeptidase activity, on the other hand, eliminates aberrant and harmful isoaspartyl peptides that arise spontaneously and accumulate in seed storage proteins. The substrate preferences differ among different plant-type enzymes. Kinetic studies revealed that the K-independent asparaginases from *L. luteus* (LlA), *E. coli* (EcAIII) and *L. japonicus* (LjNSE2) have (*in vitro*) dominating isoaspartyl aminopeptidase activity and only secondary L-asparaginase activity (Borek *et al.*, 2004; Credali *et al.*, 2011). The K-dependent enzyme from *L. japonicus* (LjNSE1) has K^+-fine-tuned L-asparaginase activity but no isoaspartyl aminopeptidase activity (Credali *et al.*, 2011). The results of Bruneau *et al.* (2006) suggested that the K-independent enzyme from *A. thaliana* has a slight preference for L-asparagine over a β-peptide, while the K-dependent enzyme from the same organism is strictly specific for L-asparagine and does not hydrolyze isoaspartyl substrates at all. Those results have recently been partly contradicted by a report that the K-independent enzyme is catalytically active with both L-Asn and β-Asp-His as substrates, while the K-dependent enzyme has a strong preference for L-asparagine over a β-peptide (Gabriel *et al.*, 2012). In the case of the human asparaginase hASNase3, kinetic studies revealed that the enzyme displays both L-asparaginase and isoaspartyl peptidase activity. However, it was able to hydrolyze L-Asp-β-methyl ester with a specificity constant that was far greater than for all other substrates tested (Cantor *et al.*, 2009). Thus, despite a significant level of structural similarity, plant-type asparaginases constitute a group of proteins with quite diversified enzymatic characteristics.

In most of the known structures of mature K-independent plant-type L-asparaginases (*e.g.* EcAIII and LlA) the nucleophilic Thr residue at the N-terminus of subunit β is positionally locked by a hydrogen bond from its free amino group to an adjacent Asn residue (Asn66 in the LlA sequence) that is a conserved element of a peculiar loop in the folding pattern of the α subunit. In the plant-type enzymes the loop conformation is stabilized by a tightly bound Na^+ cation that has an octahedral coordination provided exclusively by main-chain C=O groups. As demonstrated in the present study, this Na position has no relation to the alkali-metal cation that is important for the activity of the K-dependent enzymes. In human aspartylglucosaminidase, the corresponding loop is stabilized by a disulfide bridge (Oinonen *et al.*, 1995).

Table 1
Details of the purification and crystallization protocols for the PvAspG1–K, PvAspG1–Na and PvAspG1–K/Na complexes.

Alkali metals are highlighted in bold.

	PvAspG1–**K**	PvAspG1–**K**/**Na**	PvAspG1–**Na**
Reagents used for purification	50 m*M* Tris pH 8.0, 20–300 m*M* imidazole, 150–500 m*M* **K**Cl		50 m*M* Tris pH 8.0, 20–300 m*M* imidazole, 150–500 m*M* **Na**Cl
Protein solution for crystallization	50 m*M* Tris pH 8.0, 1 m*M* TCEP, 150 m*M* **K**Cl, protein concentration 20 mg ml^{-1}		50 m*M* Tris pH 8.0, 1 m*M* TCEP, 150 m*M* **Na**Cl, protein concentration 20 mg ml^{-1}
L-Aspartate salt added (molar excess)	**K**-Asp (1:3)	**Na**-Asp (1:25)	**Na**-Asp (1:25)
Crystallization conditions	100 m*M* bis-tris propane pH 8.5, 20%(*w*/*v*) PEG 3350, 200 m*M* **Na**NO_3		
Cryoprotection	—	2*M* **Na**NO_3	2*M* **Na**NO_3

Table 2
Apparent kinetic parameters of recombinant PvAspG1 determined in the presence or absence of 50 m*M* KCl.

	K_m (m*M*)	V_{max} ($\times10^{-8}$ mol s^{-1} mg^{-1})	V_{max}/K_m ($\times10^{-8}$ mol s^{-1} mg^{-1} m*M*$^{-1}$)	k_{cat} (s^{-1})
With K^+†	3.71 ± 1.11	57.1 ± 8.6	15.8 ± 2.2	20.4 ± 3.1
Without K^+†	9.66 ± 0.80	13.9 ± 1.0	1.44 ± 0.09	4.96 ± 0.36
ANOVA‡ *p* value	0.002	0.001	0.0004	0.001
LSD§	2.06	18.9	5.65	6.75

† $n = 3$; average ± standard deviation. ‡ Analysis of variance. § Fisher's protected least significant difference (LSD) at $p \leq 0.05$.

In this paper, we present the crystal structure of a K-dependent L-asparaginase from *Phaseolus vulgaris* (PvAspG1) in complex with different alkali-metal cations and show that, in addition to the Na^+ binding site shared with the K-independent enzymes, there is another metal site that controls the conformation of a structural motif with a key Arg residue that is responsible for the proper recognition and docking of a substrate molecule. The productive conformation of this element observed in the presence of K^+ cations is switched off when the cation is exchanged for Na^+, thus explaining the potassium dependence of the catalytic mechanism. These conclusions are based on comparative analyses of three crystal structures of the PvAspG1 protein presented in this paper. The crystals were grown from protein preparations obtained using identical procedures, except for the presence of different alkali-metal cations. The structure of PvAspG1 is therefore presented in three variants, designated PvAspG1–K (model with potassium cations), PvAspG1–Na (model with sodium cations) and PvAspG1–K/Na (model with both cations). The structures were determined at resolutions ranging from 1.79 Å for PvAspG1–K/Na to 2.30 Å for PvAspG1–K.

2. Materials and methods

2.1. Cloning, expression and purification

A full-length *PvAspG1* cDNA was cloned by RT-PCR from total RNA isolated from developing seeds of the Mesoamerican *P. vulgaris* cultivar AC Compass (Park & Rupert, 2000). The isolated cDNA has the sequence of the transcript with accession No. Phvul.001g025000.1 (corresponding to an Andean bean genotype G19833) in the early-release genome of the common bean (*P. vulgaris* v_1.0, DOE-JGI and USDA-NIFA; http://www.phytozome.org/commonbean), except that Thr is coded at position 17 instead of Asn. RNA was extracted using an LiCl precipitation method (Bruneau *et al.*, 2006). 2 µg of RNA were treated with 2 U of amplification-grade DNase I (Life Technologies Inc., Burlington, Ontario, Canada) according to the manufacturer's protocol. The Superscript First-Strand cDNA Synthesis System for RT-PCR was used to synthesize cDNA from 1 µg of RNA. The *PvASPG1* cDNA was amplified by PCR using *Pfx50* DNA polymerase (Life Technologies Inc.) and the primers 5′-CTACCCATGGGAGGTTGGGCAATTG-3′ and 5′-GTAGTCTAGATTAATCCCAAATTGCAACC-3′ designed to introduce *Nco*I and *Xba*I restriction sites at the respective 5′ and 3′ ends of the cDNA. The PCR product was cloned into the pCR BluntII TOPO vector and transformed into *E. coli* TOP10 cells (Life Technologies Inc.) for cultivation in LB medium containing 50 mg l^{-1} kanamycin. Plasmid DNA was extracted and digested with *Nco*I and *Xba*I. The insert was verified by sequencing and subcloned at the corresponding sites in the polylinker of bacterial expression vector pProExHTb (Life Technologies Inc.). The protein construct contains an N-terminal His-tag sequence, which, when cleaved by TEV protease, leaves two additional amino-acid residues at this end of the protein. Expression in *E. coli* BL21(DE3) cells was induced with 0.5 m*M* IPTG and carried out in LB medium with ampicillin at 100 µg ml^{-1} concentration at 28°C and 240 rev min^{-1} for 5 h. Cell disruption was achieved by sonication. The purification process consisted of the following steps: (i) His-trap affinity chromatography, (ii) digestion by TEV protease combined with dialysis (the TEV protease is labelled with a permanent His tag), (iii) a second His-trap affinity chromatography to remove undigested protein, the protease and His-tag debris and (iv) size-exclusion chromatography as a polishing step (Supplementary Fig. S1[1]). The chemicals used in the purification process are listed in Table 1. After the purification procedure, the protein solution was concentrated to 20 mg ml^{-1}. All purification stages were checked by SDS–PAGE, which revealed the presence of mature PvAspG1, *i.e.* autocatalytically cleaved into subunits α

[1] Supporting information has been deposited in the IUCr electronic archive (Reference: DZ5329).

Table 3
Data-collection and structure-refinement statistics.

Values in parentheses are for the last resolution shell.

	PvAspG1–K	PvAspG1–Na	PvAspG1–K/Na
PDB code	4pu6	4pv3	4pv2
Data collection			
Radiation source	BL14.2, BESSY Berlin	BL14.2, BESSY Berlin	BL14.2, BESSY Berlin
Wavelength (Å)	0.918	0.918	0.827
Temperature of measurements (K)	100	100	100
Space group	$P2_12_12_1$	$P2_12_12_1$	$P2_12_12_1$
Unit-cell parameters (Å)	a = 56.94, b = 102.67, c = 127.04	a = 57.40, b = 103.42, c = 124.56	a = 56.88, b = 102.63, c = 123.75
Crystal mosaicity (°)	0.24	0.38	0.21
Resolution range (Å)	47.60–2.30 (2.43–2.30)	46.55–2.09 (2.21–2.09)	38.77–1.79 (1.89–1.79)
Oscillation step (°)	0.5	0.5	1.0
No. of images	370	540	100
Reflections collected	239668 (27620)	481561 (76242)	280364 (44366)
Unique reflections	32518 (4237)	44381 (7009)	68445 (10836)
Completeness (%)	96.3 (78.8)	99.6 (99.0)	99.1 (98.2)
Multiplicity	7.37 (6.52)	10.85 (10.88)	4.10 (4.09)
$\langle I/\sigma(I)\rangle$	22.97 (1.98)	15.78 (2.47)	16.33 (1.98)
$R_{\rm merge}$†	0.067 (0.903)	0.104 (0.973)	0.053 (0.630)
Refinement			
Refinement program	*PHENIX*	*REFMAC*5	*PHENIX*
Independent functional protein molecule in asymmetric unit	1 molecule = $(\alpha\beta)_2$	1 molecule = $(\alpha\beta)_2$	1 molecule = $(\alpha\beta)_2$
Matthews coefficient (Å^3 Da^{-1})	2.68	2.67	2.61
TLS groups [chain *A*/*B*/*C*/*D*]	22 [4/7/6/5]	4 [1/1/1/1]	29 [9/8/5/7]
Reflections in working/test set	31509/1009	43451/930	67213/1232
R‡/$R_{\rm free}$§ (%)	17.59/23.13	17.80/23.14	16.35/20.66
No. of atoms			
Protein	4234	4240	4286
H_2O	114	286	421
K^+	4	0	4
Na^+	0	4	4
R.m.s. deviations from ideal			
Bond lengths (Å)	0.018	0.019	0.019
Bond angles (°)	1.47	1.79	1.37
$\langle B\rangle$ (Å^2)			
Protein	54.2	44.9	30.6
H_2O	42.4	47.2	37.4
K^+	48.0	—	36.3
Na^+	—	42.3	21.3
Residues in Ramachandran plot			
Favoured (%)	94.89	97.00	97.18
Allowed (%)	5.11	3.00	2.82

† $R_{\rm merge} = \sum_{hkl}\sum_i |I_i(hkl) - \langle I(hkl)\rangle|/\sum_{hkl}\sum_i I_i(hkl)$. ‡ $R = \sum_{hkl}\big||F_{\rm obs}| - |F_{\rm calc}|\big|/\sum_{hkl}|F_{\rm obs}|$, where $F_{\rm obs}$ and $F_{\rm calc}$ are the observed and calculated structure factors, respectively. § $R_{\rm free}$ is calculated in the same way as R but for the test reflections, which were randomly selected and excluded from the refinement.

(21.0 kDa) and β (13.6 kDa), in the isolation step (Supplementary Fig. S1). Moreover, in the purification stage we initially noticed proteolytic degradation of the α subunit, which was prevented by shortening the purification procedure and by the addition of L-aspartate.

2.2. Kinetic analysis of PvAspG1

For the determination of catalytic activity in the presence or the absence of K^+, the PvAspG1 protein was produced as described above except that the polishing step by size-exclusion chromatography was omitted. Four cycles of concentration and desalting in 50 m*M* Tris–HCl pH 7.4 were performed as described by Gabriel *et al.* (2012). Assays were performed as described by Bruneau *et al.* (2006) and Gabriel *et al.* (2012) using a spectrophotometric coupled-enzyme assay in 200 m*M* Tris–HCl pH 8.0 with and without 50 m*M* KCl (Table 2). The asparagine concentration ranged between 0.3 times to three times the $K_{\rm m}$ value. There was a linear relationship between product formation and time or amount of enzyme. One-way analysis of variance (ANOVA) was performed with *SAS* v.9.2 (Toronto, Ontario, Canada).

2.3. Crystallization

Prior to crystallization, the protein solution was mixed with an L-aspartate salt to produce an enzyme–product complex and to stabilize the protein by preventing proteolytic trimming of the α subunit. The protein–ligand mixture contained only potassium cations in the case of PvAspG1–K, only sodium cations in the case of PvAspG1–Na and contained both cations (potassium and sodium) in the case of PvAspG1–K/Na (Table 1). These three protein–ligand mixtures were the basis for the production of three types of crystals. The successful crystallization conditions consisted of 100 m*M* bis-tris propane pH 8.5, 20%(*w*/*v*) PEG 3350, 200 m*M* $NaNO_3$. Crystallization

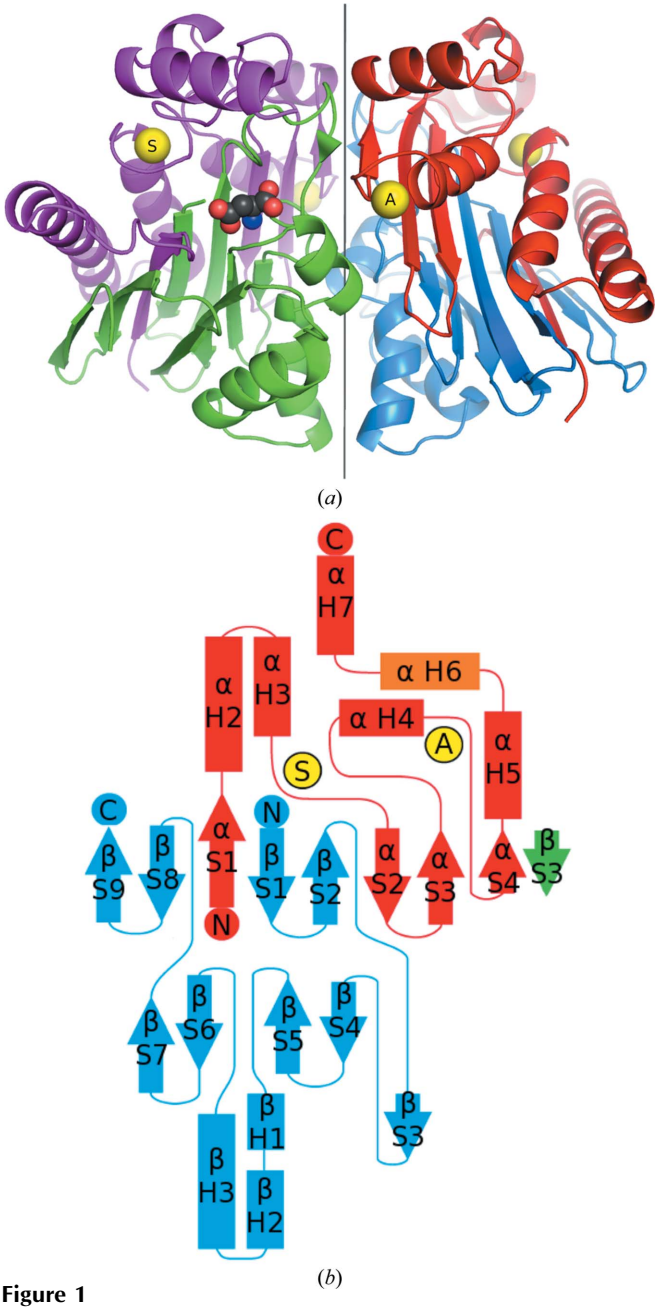

Figure 1
Overall fold of PvAspG1. (*a*) Cartoon representation of the quaternary structure with subunits α shown in pink (chain *A*) and red (chain *C*) and subunits β in green (chain *B*) and blue (chain *D*). The four yellow spheres represent the coordinated metal cations. The location of one of the active sites (in heterodimer *AB*) is marked by the reaction product molecule (L-Asp), modelled with grey, blue and red spheres for C, N and O, respectively. Note that the marked active site is placed between two metal-coordinating loops: the stabilization loop (S) in the same $\alpha\beta$ heterodimer and the activating loop (A) in the complementary $\alpha\beta$ heterodimer of the tetrameric enzyme. The *AB* and *CD* heterodimers of the enzyme are related by a noncrystallographic dyad shown as a vertical line. (*b*) Topology diagram of the ($\alpha\beta$) heterodimer formed by subunit α (red) and subunit β (blue) with the two metal-binding loops marked by yellow spheres as in (*a*) (S, stabilization loop; A, activation loop). The β-strands (S) and helices (H) are numbered following the pattern established for LlA (Michalska *et al.*, 2006), with additional labels (α, β) distinguishing the subunits. Orange colour indicates a 3_{10}-helix. The green strand extending the larger β-sheet is contributed by the complementary heterodimer. The missing αH1 element corresponds to a 3_{10}-helix found only in EcAIII.

drops were mixed with precipitant solution in a 1:1 volume ratio. All crystals were grown by the sitting-drop vapour-diffusion method at 19°C.

2.4. Data collection and processing

X-ray diffraction data for all three crystals were collected using the BL14.2 beamline at the BESSY synchrotron. Crystals were flash-cooled at 100 K in a cold nitrogen-gas stream without additional cryoprotection or with sodium nitrate as a cryoprotectant (Table 1). The diffraction data were indexed, integrated and scaled using *XDS* (Kabsch, 2010). Table 3 gives the data-collection and processing statistics.

2.5. Structure determination and refinement

The structure of the PvAspG1–K crystal was solved by molecular replacement using *Phaser* (McCoy *et al.*, 2007) with *L. luteus* L-asparaginase (LlA) as the search model (PDB entry 2gez). The protein sequence was changed to that of PvAspG1 in *ARP*/*wARP* (Langer *et al.*, 2008). The structures of the PvAspG1–Na and PvAspG1–K/Na crystals were also solved by molecular replacement but with PvAspG1–K as the search model. Manual model rebuilding according to electron-density maps was performed for all three structures in *Coot* (Emsley & Cowtan, 2004). Maximum-likelihood refinement of the PvAspG1–K and PvAspG1–K/Na structures was carried out in *PHENIX* (Adams *et al.*, 2010) and that for PvAspG1–Na in *REFMAC*5 (Murshudov *et al.*, 2011) from the *CCP*4 suite (Winn *et al.*, 2011). The TLS parameters used in the refinement were selected based on *TLSMD* analysis (Painter & Merritt, 2006*a*,*b*) or simply by assigning one group per polypeptide chain (Table 3). In the PvAspG1–K structure, the presence of the L-aspartate ligand in one of the active sites was clearly visible in the difference electron-density map generated with phases calculated from the protein model only. Moreover, four potassium ions were modelled in this structure on the basis of unusually high electron-density peaks and the number of ligand groups, which was too high for water molecules. The identification of the metal cations in the PvAspG1–K structure facilitated the assignment of the metal sites in the PvAspG1–Na and PvAspG1–K/Na structures. Furthermore, water molecules (and also nitrate ions in the case of PvAspG1–K/Na) were included in the final models according to difference electron density and stereochemical criteria. The refinement statistics are given in Table 3.

2.6. Auxiliary software

Structural figures were prepared in *PyMOL* (DeLano, 2002). Structural models of PvAspG1 were superposed using the *SSM* tool in *Coot* (Krissinel & Henrick, 2004); other structural superpositions were analyzed using *ALIGN* (Satow *et al.*, 1986). Protein sequences were aligned using *BLAST* (Altschul *et al.*, 1997; http://blast.ncbi.nlm.nih.gov/Blast.cgi).

Table 4
Model composition of the three crystal structures presented in this work.

Feature	Chain	PvAspG1–K	PvAspG1–Na	PvAspG1–K/Na
Residues modelled in electron density	*A*	2–158	2–158	2–156
	B	196–326	196–326	196–326
	C	2–158	2–156	2–159
	D	196–326	196–326	196–326
Metal cation in stabilization loop (occupancy)	*A*	K (1.0)	Na (1.0)	K/Na (0.3/0.7)
	C	K (1.0)	Na (1.0)	K/Na (0.3/0.7)
Metal cation in activation loop (occupancy)	*A*	K (1.0)	Na (1.0)	K/Na (0.3/0.7)
	C	K (1.0)	Na (1.0)	K/Na (0.3/0.7)
Small molecules in active site (occupancy)	*B*	L-Aspartate (0.7)	A few water molecules	A few water molecules
	D	A few water molecules	A few water molecules	A few water molecules

Table 5
R.m.s. deviations (Å) for pairwise superpositions of selected fragments of the PvAspG1–K, PvAspG1–Na and PvAspG1–K/Na structures.

Superposition	PvAspG1–K *versus* PvAspG1–Na	PvAspG1–Na *versus* PvAspG1–K/Na	PvAspG1–K/Na *versus* PvAspG1–K
C^{α} atoms of complete $(\alpha\beta)_2$ molecules	0.44	0.32	0.41
All atoms of the stabilization-loop area (chain *A*, residues 55–71)	0.22	0.16	0.18
All atoms of the activation-loop area (chain *C*, residues 108–121)	0.38	0.17	0.27

3. Results

3.1. Potassium dependence of PvAspG1

The potassium dependence of PvAspG1 was confirmed by determining apparent kinetic parameters with L-asparagine, in the presence or absence of 50 m*M* KCl, after extensive desalting to remove monovalent cations. Addition of K^+ resulted in a 2.5-fold decrease in the apparent K_m value and an approximately fourfold increase in the apparent V_{max} value (Table 2). Overall, the catalytic efficiency increased by 11-fold in the presence of K^+. These results are similar to those obtained with LjNSE1 (Credali *et al.*, 2011).

3.2. Overall structure of PvAspG1

Like all other plant-type L-asparaginases, the PvAspG1 enzyme from *P. vulgaris* arises from two copies of a precursor protein, which both undergo identical autoproteolytic cleavage into subunits α and β (Supplementary Fig. S1). The mature protein used in the present studies therefore consists of four polypeptide chains assembled as an $(\alpha\beta)_2$ heterotetramer or dimer of heterodimers (Fig. 1*a*). The α subunits have chain labels *A* and *C* and the β subunits are labelled *B* and *D*. The quaternary structure is stabilized by many hydrogen bonds and other interactions between all four subunits. The *AB* and *CD* heterodimers of the enzyme are related by a noncrystallographic twofold axis (Fig. 1*a*). The $\alpha\beta$ heterodimer has a classical Ntn-hydrolase sandwich fold (Fig. 1*b*). The core of the heterodimer is formed by two almost exclusively antiparallel β-sheets. The core β structure is flanked on both sides by layers of helices. There are six helices (H) in subunit α (αH2, αH3, αH4, αH5, αH6 and αH7) and three helices in subunit β (βH1, βH2 and βH3). The smaller β-sheet is comprised of four strands (S) from subunit β (βS7, βS6, βS5 and βS4). The larger β structure consists of eight β-strands contributed by both subunits (βS9, βS8, αS1, βS1, βS2, αS2, αS3 and αS4) and an additional strand from subunit β of the complementary heterodimer (βS3; Fig. 1*b*). The large β-sheet is therefore the centre of cohesion not only for one heterodimer but for the entire tetrameric assembly. The N-terminus of subunit β is embedded in the large β structure and marks the location of the active site. The PvAspG1 enzyme has two active sites, one in each β subunit.

There are two distinct metal-binding sites in each α subunit. The entire K-dependent enzyme therefore coordinates four metal cations. The metal-binding sites are situated in extended loops, in each case linking an α-helix with the following β-strand. The loop known as the sodium-binding loop of the K-independent enzymes, formed between helix αH3 and strand αS2, is also present in the K-dependent protein and is referred to here as the stabilization loop. The other metal-binding loop, formed between helix αH4 and strand αS4, is a novel feature of this enzyme and will be referred to as the activation loop. The active site of one heterodimer (*e.g. AB*) is situated between the stabilization loop from the same heterodimer (*AB*) and the activation loop from the other heterodimer (*CD*) (Fig. 1*a*). It is important to keep these features of the PvAspG1 topology in mind as they are essential for the discussion below.

3.3. Comparison of the three models of PvAspG1

All three PvAspG1 L-asparaginase crystal forms were grown from protein material that originated from the same coding sequence and was prepared using the same expression, purification and crystallization procedure. All of the crystals are isomorphous and the asymmetric unit in all cases contains one complete protein molecule, *i.e.* a heterotetrameric $(\alpha\beta)_2$ assembly. The three structures contain variable numbers of water molecules, reflecting the level of resolution. The PvAspG1–K/Na model contains additional nitrate ions (from the crystallization buffer) in the solvent area, which could be modelled owing to the superior resolution of this structure. The three models include different metal cations: potassium cations in PvAspG1–K, sodium cations in PvAspG1–Na and potassium and sodium cations in PvAspG1–K/Na.

The mature full-length PvAspG1 protein is comprised of amino-acid residues 1–195 (subunit α) and 196–326 (subunit β). The protein construct used in this work contains two extra residues (numbered −1 and 0) at the N-terminus of subunit α,

which were introduced as a cloning artifact. In all three PvAspG1 structures all of the β subunits contain the complete sequence (Table 4) modelled without ambiguity in the electron-density maps. All of the α subunits lack some amino-acid residues that could not be modelled because of disorder. These are residues −1, 0 and 1 at the N-terminal ends and between 36 and 39 residues at the C-terminal ends of the α subunits (Table 4). The C-terminal peptide of subunit α forms the inter-domain linker of the immature protein and is liberated upon the autoproteolytic event. This fragment is sometimes called a variable loop because it is the most diversified (in sequence and length) fragment of plant-type L-asparaginases. It is also speculated to have a role as a determinant of substrate preference (Gabriel *et al.*, 2012). Unfortunately, it is often disordered (for example in LlA; Michalska *et al.*, 2006) or even degraded (for example in EcAIII; Borek *et al.*, 2004) in the crystal structures. In this work, proteolytic trimming was initially observed at the purification stage. However, this degradation could be prevented (as documented by SDS–PAGE; not shown) by minimizing the duration of the purification procedure and by addition of the Asp ligand to the protein material before crystallization. Nevertheless, despite the preservation of the C-terminus of the α subunit, we were unable to model the variable loop because of a lack of adequate electron density.

A superposition of the C^{α} atoms of the three models is characterized by r.m.s. deviations of less than 0.5 Å, suggesting that overall they are very similar (Table 5). However, on closer inspection there are several areas of divergence that mostly locate to flexible surface elements, *e.g.* loops or helices between residues Gly13–Gln23, Leu72–Val78, Pro145–

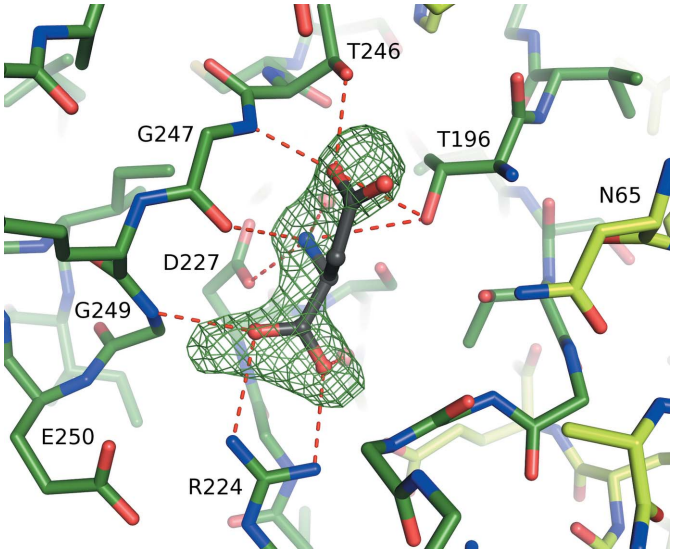

Figure 2
Interactions within the active site. The active site of PvAspG1–K, with chain *A* (α) shown as light green sticks and chain *B* (β) shown as dark green sticks, occupied by L-Asp (grey ball-and-stick representation) in an $F_o - F_c$ OMIT map contoured at 2.5σ. Residues forming interactions with the ligand molecule and some other components of the active-site environment are labelled. Hydrogen bonds between the ligand and protein residues are indicated by red dashed lines. Red spheres represent water molecules.

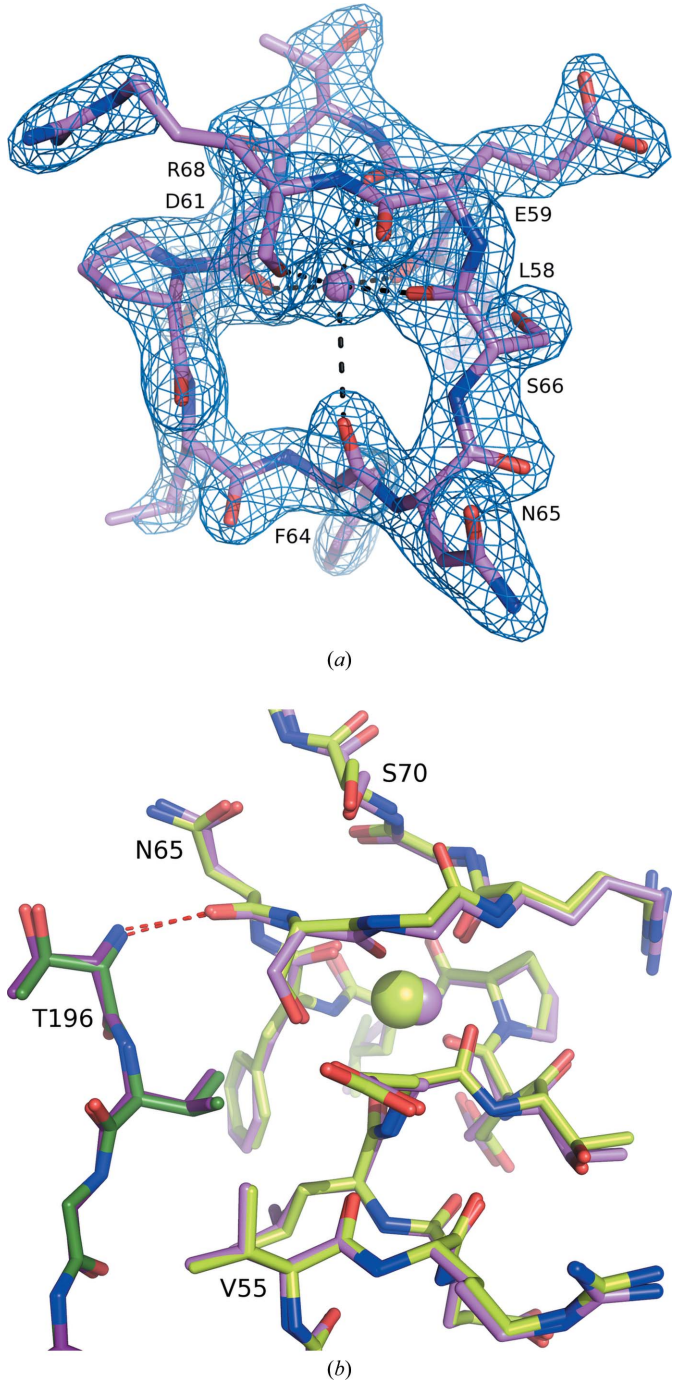

Figure 3
The stabilization loop. (*a*) Representation of the stabilization loop of PvAspG1–Na chain *A* (violet sticks with atoms coloured blue for N and red for O) with coordination bonds (black dashed lines) between the Na^{+} cation (violet sphere) and six carbonyl groups arranged in an octahedron. The model is shown as $2F_o - F_c$ electron density contoured at 2.0σ. (*b*) Superposition of the stabilization-loop areas of PvAspG1–Na (chain *A*, light violet sticks; chain *B*, dark violet sticks) with sodium (light violet sphere) and PvAspG1–K (chain *A*, light green sticks; chain *B*, dark green sticks) with potassium (light green sphere), including additional (anchoring) residues at both ends (Val55–Ser70) of the loop. Note that the two superposed loops have exactly the same conformation, including side chains, despite the different ionic radii of the two metal cations (drawn to scale). The picture also illustrates the stabilizing hydrogen bond (red dashed line) between Asn65 from the loop sequence and the catalytic Thr196.

Table 6
Potential hydrogen bonds within the active site of PvAspG1–K (heterodimer *AB*).

Residue	Interacting atoms	Interacting partner	Distance (Å)
Aspartate ligand	N···$O^{\delta1}$	Asp227	2.8
	N···O	Water	2.9
	N···O	Gly247	3.2
	N···$O^{\gamma1}$	Thr196	3.3
	O···$N^{\eta1}$	Arg224	2.8
	O···O	Water	3.1
	OXT···N	Gly249	2.8
	OXT···$N^{\eta2}$	Arg224	3.0
	$O^{\delta1}$···O	Water	2.9
	$O^{\delta2}$···N	Gly247	2.5
	$O^{\delta2}$···$O^{\gamma1}$	Thr246	2.6
	$O^{\delta2}$···$O^{\gamma1}$	Thr196	3.0
Thr196	$O^{\gamma1}$···N	Thr196	2.9
	$O^{\gamma1}$···$O^{\gamma1}$	Thr214	2.7
	N···O	Asn65	2.8
	N···O	Water	3.0
	O···O	Water	3.5
	O···N	Gly11	2.9
Arg224	$N^{\eta1}$···O	Water	3.0
	$N^{\eta2}$···$O^{\varepsilon2}$	Glu250	3.3
	N^{ε}···$O^{\varepsilon1}$	Glu250	3.1
	N^{ε}···O	Water	3.4

Asn158, Met218–Gly223 and Leu270–Lys288. Some of these regions have clear importance for the enzyme activity and will be discussed in detail below.

3.4. The architecture of the active site

Each active site, marked by the Thr196 residue at the N-terminus of subunit β, is located at the edge of the large β-sheet. The active-site pocket, which is nested between the two β-sheets, has a funnel shape and is sculpted mainly by several loops from both subunits (α and β) that connect the helical layers with the β-sheets. Thr196, which is the catalytic nucleophile in the asparaginase reaction, is also proposed to act as the nucleophile during the autocatalytic cleavage of the protein-maturation process.

Of the three structures presented here, only PvAspG1–K has one of the active sites occupied by the reaction product (L-aspartate), which was modelled with occupancy of 0.7. The partial occupancy of the bound L-aspartate is probably a consequence of a relatively low molar excess of the ligand (1:3) in the crystallization buffer. The unintended difference in ligand occupation of the two active sites of PvAspG1–K is actually a benefit because it can be used to address the question of ligand influence on the active-site conformation. There is no trace of L-aspartate in any of the active sites in the crystal structures of PvAspG1–Na and PvAspG1–K/Na, despite the fact that these crystallization experiments were carried out with a 25-fold molar excess of sodium aspartate. The presence of elevated levels of sodium ions in the crystallization conditions evidently reduced the ability of the protein to bind L-aspartate.

The molecule of L-aspartate found in the active site of PvAspG1–K does not fill the whole cavity, leaving an empty space at the extension of the side chain (adjacent to the amide N atom of the L-asparagine substrate) that is sufficiently large to accommodate the second residue of an isoaspartyl substrate. This second residue of an isoaspartyl dipeptide would be bound by the α subunit or, more specifically, by a

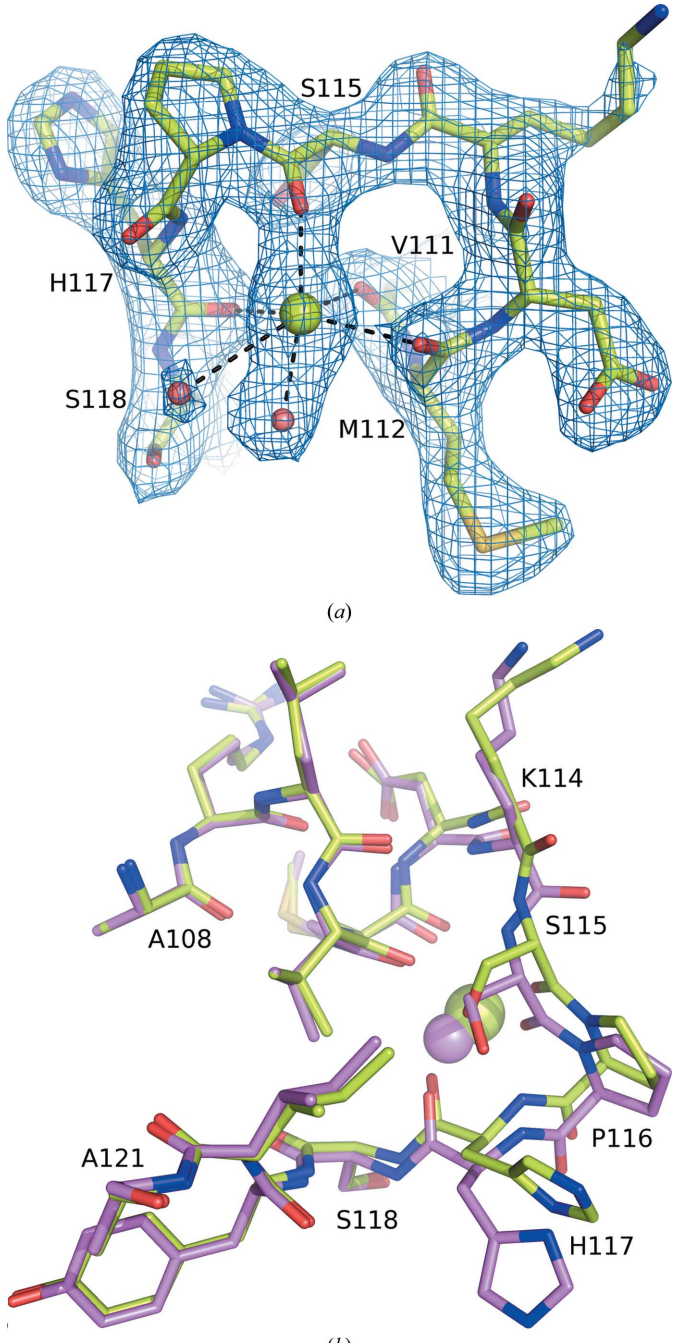

Figure 4
The activation loop. (*a*) Representation of the activation loop of PvAspG1–K chain *C* (green sticks with atoms coloured blue for N, red for O and yellow for S) with coordination bonds (black dashed lines) between the K^+ cation (green sphere) and the carbonyl groups of four residues and two water molecules (red spheres). The model is shown as $2F_o - F_c$ electron density contoured at 2.0σ. (*b*) Superposition of the activation-loop areas (chains *C*) of PvAspG1–Na (violet sticks) with sodium (violet sphere) and PvAspG1–K (green sticks) with potassium (green sphere), including additional (anchoring) residues at both ends (Ala108–Ala121) of the loop. Note the variability of the main-chain trace and the completely different conformation of His117, which is an element of the catalytic switch.

Table 7
Metal coordination in the stabilization loops.

The ligand atoms have been selected using stereochemical criteria: shortest metal···O distances with octahedral geometry. Occasional long (∼3.3 Å) distances (*e.g.* to water molecules) have been omitted. Isotropic *B* factors (Å^2) of the metal ions and ligand atoms are given in parentheses.

	PvAspG1–K		PvAspG1–Na	
	Chain *A*: K (41.7) Chain *C*: K (57.8)		Chain *A*: Na (40.2) Chain *C*: Na (40.8)	
Ligand residue	Ligand atom	Distance (Å)	Ligand atom	Distance (Å)
Leu58	O (37.1)	2.93	O (39.2)	2.96
	O (47.7)	2.85	O (36.7)	2.84
Glu59	O (29.4)	2.95	O (38.4)	2.60
	O (47.8)	2.86	O (40.5)	2.55
Asp61	O (42.0)	2.52	O (31.1)	2.27
	O (50.6)	2.58	O (33.4)	2.27
Phe64	O (29.5)	3.10	O (39.6)	3.32
	O (49.9)	3.19	O (33.6)	3.20
Ser66	O (25.4)	2.64	O (31.5)	2.35
	O (43.4)	2.62	O (33.3)	2.23
Arg68	O (31.1)	2.56	O (30.1)	2.23
	O (36.1)	2.66	O (32.1)	2.33

loop with a characteristic GAG motif (Michalska & Jaskolski, 2006) consisting of Gly11, Ala12 and Gly13.

A comparison of the occupied and the empty active sites of PvAspG1–K shows no significant rearrangement of the surrounding residues. The L-Asp reaction product is anchored in the active site by hydrogen bonds to the β subunit only. The docking is established by five residues and three water molecules (Fig. 2, Table 6). The α-carboxy group of the product molecule interacts with the main-chain N atom of Gly249 and with the guanidinium group of Arg224. The α-amino group forms hydrogen-bond interactions with the side chain of Asp227 and with the main-chain carbonyl O atom of Gly247. The hydroxyl group of Thr246 and the amide NH group of Gly247 form interactions with the β-carboxylate group in a way that makes them very likely to be components of the oxyanion hole that stabilizes the negative charge developing on the O atom of the substrate during the catalytic reaction. All of these points of attachment are identical to those reported for docking of the L-Asp product in the active site of K-independent plant-type L-asparaginases (Michalska *et al.*, 2005; Nomme *et al.*, 2012).

A comparison of the architecture of the active sites of PvAspG1–K with those found in the PvAspG1–Na and the PvAspG1–K/Na complexes shows only one (but a very significant) difference, in the orientation of the side chain of Arg224, which is the docking site for the α-carboxy group of the product/substrate. This aspect is described in detail in §3.7.

3.5. The stabilization loop

The stabilization loop, residues Leu58–Arg68 (Fig. 3), contributes to the stability of the active site *via* a hydrogen bond between the free α-amino group of the catalytic Thr196 nucleophile and the main-chain carbonyl group of Asn65 (Fig. 3*b*). This interaction is essential for the proper orientation of the Thr196 residue for nucleophilic attack on the substrate amide group during the catalytic reaction. The

Table 8
Metal coordination in the activation loops.

Isotropic *B* factors (Å^2) of the metal ions and ligand atoms are given in parentheses.

	PvAspG1–K		PvAspG1–Na	
	Chain *A*: K (44.9) Chain *C*: K (47.8)		Chain *A*: Na (44.4) Chain *C*: Na (43.9)	
Ligand residue	Ligand atom	Distance (Å)	Ligand atom	Distance (Å)
Val111	O (37.2)	2.97	O (27.9)	2.69
	O (36.6)	2.87	O (32.3)	2.70
Met112	O (41.9)	2.89	O (36.7)	3.38
	O (37.3)	2.80	O (42.8)	3.10
Ser115	O (39.7)	2.65	O (41.7)	2.44
	O (34.2)	2.45	O (42.9)	2.40
His117	O (42.3)	2.70	O (36.2)	2.34
	O (36.2)	2.67	O (37.4)	2.61
Wat	O (33.6)	2.55	O (36.7)	2.23
	O (28.1)	2.46	O (35.1)	2.28
Wat	O (55.6)	2.99	O (34.5)	2.34
	O (41.9)	3.42	O (49.4)	3.21

stabilization loop, located at the end of helix αH3 of subunit α, is built of 11 residues and revolves 1.5 times around the metal ion coordinated at its centre. The coordination sphere of the central atom has octahedral geometry but is very unusual as a specific metal-binding element because all of the metal–O coordination bonds are formed exclusively by main-chain carbonyl groups, with the side chains flipped out of the loop.

The two stabilization loops in the PvAspG1–K structure, one located in chain *A* and one in chain *C*, are occupied by potassium cations and have octahedral geometry, with sporadic additional longer contacts (Table 7). The same two sites in the PvAspG1–Na structure are occupied by sodium cations and also have octahedral geometry (Fig. 3*a*, Table 7). In the PvAspG1–K/Na structure the metal sites in the stabilization loops have mixed occupancy, with potassium and sodium sharing each site in a 3:7 ratio and with quite diversified coordination bonds.

A superposition of all of the stabilization loops in the presented structures shows no significant difference in their general shape (Table 5). However, the position of the sodium cations (PvAspG1–Na) is shifted by ∼0.5 Å with respect to the potassium cations (PvAspG1–K) (Fig. 3*b*), while the partial ions in PvAspG1–K/Na are even farther apart (∼1.9 Å). Therefore, we conclude that the stabilization loop of PvAspG1 can utilize different available alkali-metal cations with no effect on its stabilizing function.

3.6. The activation loop

The term 'activation loop' reflects the fact that it activates, as described below, a catalytic switch mechanism of the mature enzyme. This loop, which is located at the end of the αH4 helix of subunit α, is formed by eight residues (Val111–Ser118) completing one full turn around the central ion. The coordination sphere around the metal cation is octahedral and is created by four main-chain carbonyl groups supplemented by two water molecules, of which at least one is fixed in the appropriate position by the side chain of Ser118, the last

residue of the activation loop (Fig. 4*a*, Table 8). This specific alkali-metal coordination by the activation loop is reported here for the first time and appears to be a characteristic feature of K-dependent plant-type L-asparaginases.

Each of the activation loops in the PvAspG1–K structure is occupied by a potassium cation and in the PvAspG1–Na structure by a sodium cation. A superposition of these structures using all C^{α} atoms shows not only a ∼1.0 Å shift in the relative ion positions but also significant changes (shifts) in the relative position of the residues forming the framework of the activation loops, even though the positions of the points of entry (N-terminus, Ala108) and exit (C-terminus, Ala121) of this loop are invariable and have an identical position in space (Fig. 4*b*, Table 5). Moreover, the conformations of the side chains of four amino-acid residues in this loop (Lys114, Ser115, Pro116 and His117) undergo changes that are correlated with the metal type coordinated in this loop.

The activation loops in the PvAspG1–K/Na structure are occupied by K^{+} (occupancy 0.3) and Na^{+} (0.7) cations, whose centres are separated by ∼1.5 Å. The dual metal occupancy is correlated with the side chain of His117, which adopts two conformations corresponding to those found in PvAspG1–K and PvAspG1–Na, populated in the same 3:7 ratio. The main-chain fold, as well as the remaining side-chain conformations, are similar to those in the PvAspG1–Na structure. We postulate that different alkali-metal cations coordinated by the activation loop influence its conformation and interactions, with consequences for the enzymatic activity.

3.7. The catalytic switch

The catalytic centre, marked by the OH group of the Thr196 nucleophile, is ∼10 Å away from the metal cation in the stabilization loop and ∼18 Å from the metal cation in the activation loop. Similarly, the C^{α} atom of the L-Asp molecule found in the active site of PvAspG1–K is ∼13 and ∼15 Å away from the former and the latter metal centres, respectively. Therefore, the metal cations coordinated in the loops cannot influence the catalytic mechanism directly. Nevertheless, the rearrangement of the activation loop effected by the exchange of the coordinated alkali-metal cation results in structural changes that are communicated to the active-site area. These changes are most pronounced in the conformation of the side chains of His117, Arg224 and Glu250, which collectively form a 'catalytic switch' that can adopt an ON or OFF state depending on the metal cation coordinated in the activation loop (Fig. 5*a*).

In the PvAspG1–K structure, the switch area is configured in a way that allows anchoring of the reaction substrate/product in the active site, and this state of the switch is defined as ON. His117, which is part of the activation loop, is located in the centre of the switch area. In the activation-loop conformation enforced by potassium coordination, the imidazole ring of His117 is directed towards the surface of the protein. Next to the His117 side chain, but located deeper within the protein core, the side chain of Arg224 is directed towards the active site, anchoring the L-aspartate with a fork of salt-bridge/hydrogen bonds between the $N^{\eta 1}$ and $N^{\eta 2}$ atoms of the guanidinium group and the α-carboxylate group of the ligand (Fig. 5*a*). The side chains of His117 and Arg224 are fixed in their catalytically competent conformation by Glu250, which forms hydrogen bonds to the guanidinium group of Arg224

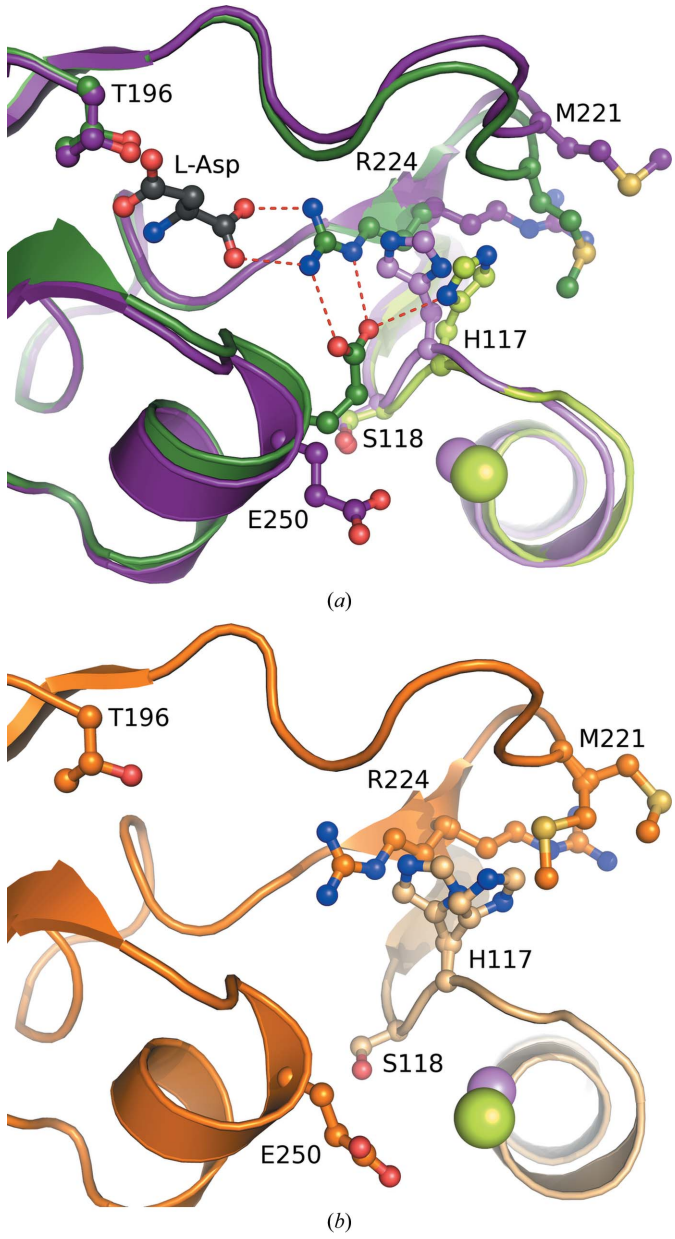

Figure 5
Switching of the catalytic apparatus. Cartoon representation of the active-site (chain *B*) and activation-loop (chain *C*) areas. Residues forming the catalytic switch (His117–Arg224–Glu250), the catalytic nucleophile (Thr196), the ligand molecule (L-Asp) and additionally residues Met221 and Ser118 are labelled and shown in ball-and-stick representation. (*a*) Superposition of the catalytic switch area of PvAspG1–Na (chain *B*, dark violet; chain *C*, light violet) with sodium (light violet sphere) in the activation loop with the catalytic switch area of PvAspG1–K (chain *B*, dark green; chain *C*, light green) with potassium (light green sphere) in the activation loop, including the molecule of L-Asp (grey ball-and-stick model) in the active site. (*b*) The catalytic switch area of PvAspG1–K/Na (chain *B*, dark orange; chain *C*, light orange) with sodium (violet sphere) and potassium (green sphere) in the activation loop, showing the double conformation of the catalytic switch residues.

and the imidazole ring of His117. The conformations of His117 and Arg224 are exactly the same in the two (L-Asp-occupied and empty) active sites of the PvAspG1–K structure. The conformation of the third element of the catalytic switch, Glu250, however, is not. In the active-site area of chain *B*, which is occupied by the reaction product, the guanidinium group of Arg224 is precisely oriented by a fork of salt-bridge/hydrogen bonds between its $N^{\eta 2}$ and N^{ε} atoms and the carboxylate group of the side chain of Glu250. There is also one hydrogen bond between Glu250 and the side chain of His117 (Fig. 5*a*). In the active-site area of chain *D*, which is empty, the conformation of Glu250 maintains its hydrogen bond to His117. However, one of the Glu250 side-chain O atoms now forms two hydrogen bonds to Arg224 (atoms $N^{\eta 2}$ and N^{ε}), while the other is anchored by two hydrogen bonds to Ser118, namely to its NH amide and side-chain OH groups. Despite the apparent differences, both conformations of Glu250 in the PvAspG1–K structure are compatible with the ON state of the catalytic switch because of their similar shape, their occupation of the same general space and their ability to create a stable environment for ligand docking, as reflected in the orientation of Arg224. It must therefore be concluded that the switch mechanism is activated by the alkali metal in the activation loop and not by the presence or absence of a ligand molecule in the active site.

A superposition of the PvAspG1–K and PvAspG1–Na structures shows how the catalytic switch residues reconfigure their side chains into the OFF position to fine-tune/switch off the enzymatic activity of the enzyme (Fig. 5*a*). When the potassium cation inside the activation loop is replaced with sodium, the loop undergoes a significant rearrangement (Fig. 4*b*). It relays the conformational changes to several side chains of amino-acid residues in its sequence, with His117 being among them. The side chain of this residue moves deeper into the protein core, taking up the space previously occupied by the side chain of Arg224. To avoid steric clashes, the side chain of Arg224 rotates ∼180° and now points in the opposite direction. In this new position, Arg224 is no longer capable of anchoring the substrate/product in the active site. Moreover, this new orientation of the Arg224 side chain nudges the residues of the preceding Met218–Gly223 loop (located above the catalytic switch), displacing the Met221 side chain to the protein surface. The side chain of Glu250 also moves away from the active site. It adopts two slightly different but generally similar conformations in the two active-site areas of the PvAspG1–Na structure. In both orientations, the Glu250 side chain no longer interacts with any other residues. In heterodimer *AB* the side chain of Glu250 forms a hydrogen bond to a water molecule, which is also in contact with the sodium cation in the activation loop, and with the Ser118 side chain. In heterodimer *CD* the side chain of Glu250 forms a hydrogen bond to a different water molecule.

The active site in the PvAspG1–K/Na structure shows an intermediate situation, correlated with the dual occupancy of the activation loops by K^+ (0.3) and Na^+ (0.7) (Fig. 5*b*). In this case, the conformation of the catalytic switch in both active-site areas is identical. The side chains of His117 and Arg224 assume both conformations, *i.e.* the ON state (as in PvAspG1–K) with 0.3 occupancy and the OFF state (as in PvAspG1–Na) with 0.7 occupancy. Glu250 has a new conformation; however, it still occupies the same area as in the OFF configuration, without any interactions with other residues. Similarly, the Met218–Gly223 loop replicates the shape and position of the PvAspG1–Na loop. The side chain of Met221 shows even more flexibility, as it adopts two new conformations, still filling the same space as in the ON and OFF states.

4. Discussion

4.1. Identification of the metal cations in the binding loops

It was technically not possible to collect anomalous signal data for potassium and sodium, and the signal at the wavelengths of the experiments, 0.918 and 0.827 Å, is very small (∼0.4e and ∼0.04e for K and Na, respectively), as confirmed by the marginal or non-existent anomalous signal indicators (d''/σ; $CC_{1/2}$) reported for all three data sets by *SHELXC* (Sheldrick, 2008). Nevertheless, we inspected the anomalous difference maps of all three crystals (Thorn & Sheldrick, 2011). For PvAspG1–Na and PvAspG1–K/Na they were featureless at the metal sites and the only (very low) possibly interpretable peaks were near S atoms. For the PvAspG1–K data set, however, four of the highest anomalous difference peaks (3–4σ) were found at the potassium sites. They were comparable in height with the peaks at S atoms. These tests, although weak, allowed us to conclude that the only structure where the presence of potassium ions at high occupancy could be detected was PvAspG1–K. Additional tests aimed at identifying the metal cations in the stabilization and activation loops had to use indirect evidence.

According to data-mining analyses, both metals prefer main-chain carbonyl O atoms rather than amino-acid side chains as their ligands, and both usually have five or six (rarely four or seven) as the coordination number (Harding *et al.*, 2010). The expected metal–ligand distances were evaluated (Harding, 2006; Harding *et al.*, 2010; Kuppuraj *et al.*, 2009) on the basis of detailed analyses of metal-ion environments found in the structures deposited in the Protein Data Bank (Berman *et al.*, 2000) and in the Cambridge Structural Database (Allen, 2002). Since the interaction between a metal cation and protein is to a significant degree electrostatic, coordination bonds are more variable in length than covalent bonds. The observed geometry and bond lengths in the coordination sphere do not only depend on the metal-ion type and its size, charge and preferred coordination number. Also important are the actual number of ligands (more ligands correlate with longer bonds) and the type of donor atoms (*e.g.* metal–water distances tend to be longer than metal–main-chain carbonyl distances). Also, the resolution of the structure determination has to be taken into account, as lower resolution results in a wider spread (and ambiguity) of the observed parameters owing to experimental error. The expected metal–main-chain O distances are 2.38 (10) Å for Na^+ and 2.74 (15) Å for K^+.

Table 9
The bond-valence test for the identification of metal ions.

R_{ij} is the bond-valence parameter, to be compared with the recommended values for metal···O bonds given in Table 5 of Brese & O'Keeffe (1991): $R_{KO}(K) = 2.13$; $R_{NaO}(Na) = 1.80$. V_i is the total valence of the central metal cation, calculated according to Brese & O'Keeffe (1991), using recommended bond-valence parameters. For correctly validated cations, the valence of the monovalent K^+ and Na^+ ions should be close to 1.0. Values in italics are hypothetical numbers calculated assuming alternative (K *versus* Na) identity of the metal ion. Each entry lists values for the stabilization/activation loops.

	PvAspG1–K	PvAspG1–Na	PvAspG1–Na/K	
Chain	*A*	*A*	*A*	
Chain	*C*	*C*	*C*	
R_{ij}	2.01/2.09	1.80/1.78	2.08/2.09 (K)	1.76/1.82 (Na)
	2.08/2.01	1.78/1.92	2.08/2.34 (K)	1.74/1.87 (Na)
Assumed cation	Total valence V_i of the central metal cation			
K^+	1.11/1.21	*2.43/2.80*	1.15/1.10 (K)	*2.71/2.32 (Na)*
	1.39/1.14	*2.55/1.76*	1.15/0.56 (K)	*2.86/2.04 (Na)*
Na^+	*0.45/0.50*	0.99/1.06	*0.47/0.45 (K)*	1.10/0.95 (Na)
	0.57/0.47	1.05/0.72	*0.47/0.23 (K)*	1.18/0.94 (Na)

The corresponding metal–water distances are 2.41 (10) and 2.81 (15) Å (Harding *et al.*, 2010). As a guide, the *B* factor of a properly identified and refined metal ion should be close to the *B* factors of its ligands (Zheng *et al.*, 2008). The bond-valence (BV) method of Brese & O'Keeffe (1991) is a useful tool for evaluating metal-ion assignments in crystal structures. Although rigorous identification usually requires accurate data at high resolution (Brown, 2009), for discrimination and comparative purposes data at ∼2 Å are sufficient, especially if they lead to consistent conclusions. Metal-binding sites in macromolecular structures can also be validated using the *CheckMyMetal* (*CMM*) web server (Zheng *et al.*, 2014).

During PvAspG1–K crystallization, potassium and sodium ions were present; thus, theoretically both cations could be present in this structure. It should be noted, however, that during all preliminary protein-handling procedures (up to crystallization) only potassium cations were used, at a level of 0.15–0.5 *M* (Table 1). Consistently, the modelling of four potassium sites gave the best interpretation of the diffraction data. The high level of the $2F_o - F_c$ electron density (4.1–6.3σ) suggests species heavier than sodium or water. The refined *B* factors of the K^+ cations are compatible with those of the ligand atoms (Tables 7 and 8). When the potassium sites were replaced with Na^+ in a test refinement, the *B* factors dropped to ∼10 Å^2 below those of the ligands (not shown). The *CMM* server favoured potassium over sodium as well (Supplementary Fig. S2). Also, the results of BV calculations (Table 9) are consistent with potassium cations. All of these numerous tests consistently and convincingly confirm the presence of potassium cations in the PvAspG1–K structure.

The protein sample and crystals of PvAspG1–Na were prepared using sodium cations only (Table 1), so the probability of the presence of other cations is very low. The $2F_o - F_c$ electron density of the four Na^+ cations in the metal-binding loops is on a par with that of water molecules (2.9–4.0σ). However, the metal–ligand distances are much shorter than water···O hydrogen bonds. The *B* factors of the sodium ions and their ligands are similar (Tables 7 and 8). The BV tests clearly confirm the presence of sodium (Table 9). When the sodium sites were replaced with K^+ in a test refinement, the *B* factors increased to ∼60 Å^2, about 20 Å^2 above those of the ligands (not shown). The *CMM* server also favoured sodium over potassium (Supplementary Fig. S2). Thus, also in this case, all of these numerous tests consistently and convincingly confirm the presence of sodium cations in the PvAspG1–Na structure.

The situation is more complicated in the PvAspG1–K/Na structure, in which the loops are in all probability occupied by both cations. This is consistent with the presence of both cations at elevated concentration during the purification and crystallization procedures (Table 1). In this case, despite the highest resolution (1.79 Å), a simple verification by electron density is not very meaningful. We have therefore modelled each of the four sites with both metals and adjusted their fractional occupancies (K^+, 0.3; Na^+, 0.7) to achieve well balanced *B* factors upon refinement, under the constraint of full combined occupation. Such a model, which to a certain degree is arbitrary (at least with respect to the proportion of occupancies and its constancy at various sites), does not contradict the diffraction data and is consistent under the BV and *CMM* tests (Table 9, Supplementary Fig. S2).

Table 10
Structural comparisons of plant-type L-asparaginases.

R.m.s. deviations (Å) for C^α superpositions calculated in *ALIGN* (Satow *et al.*, 1986). The following PDB models were selected for comparison with PvAspG1–K: *E. coli* asparaginase III (EcAIII), PDB entry 2zal (the highest degree of completeness, L-Asp bound in the active site, resolution 1.9 Å); *H. sapiens* asparaginase III (hASNase3), PDB entry 4gdw (the only model of fully mature protein, L-Asp in the active site, resolution 1.84 Å); *L. luteus* asparaginase (LlA), PDB entry 2gez (the only available model of a genuine plant K-independent asparaginase, resolution 1.9 Å).

	LlA (2gez)	EcAIII (2zal)	hASNase3 (4gdw)
PvAspG1–K	0.61	0.90	1.02
LlA (2gez)		0.82	0.96
EcAIII (2zal)			1.03

4.2. Comparison of different plant-type L-asparaginases

Plant-type asparaginases are divided into potassium-dependent and potassium-independent enzymes, although plant proteins belonging to both groups show a relatively high level of sequence similarity and identity (∼70 and ∼60%, respectively), in contrast to homologous L-asparaginases from other organisms, for which the identity level is reduced to 40% (Supplementary Table S1). The amino-acid sequences within the K-dependent group are remarkably consistent (∼90%). For example, the PvAspG1 and LjNSE1 sequences (both 326 residues in length) have only 29 different residues, of which 15 are similar. A comparison of the four known plant-type L-asparaginase structures revealed that PvAspG1 is most similar to LlA (Table 10), which is not surprising as both proteins are of plant origin, in contrast to the bacterial (EcAIII) or human (hASNase3) homologues.

Despite the differences in amino-acid sequence between the *P. vulgaris* K-dependent enzyme and other plant-type

L-asparaginases, all of these structures have a very similar fold. Also, their quaternary structure is supported by essentially the same interactions. The topology diagram of the $\alpha\beta$ heterodimer of PvAspG1 (Fig. 1*b*) is exactly the same as that of LlA (Michalska *et al.*, 2006), while EcAIII has two additional secondary structures (αH1 and βH4; Michalska *et al.*, 2005). In hASNase3, the larger β-sheet consists of the same number of strands (nine), but βS3 (at one end) is missing, while (at the other end) an extra βS10 strand (labelled M) is present that is formed to accommodate a nine-residue insertion in the β-subunit sequence (Nomme *et al.*, 2012). The presence (or absence) of the βS3 strand is somewhat debatable as it may not be detected by automatic secondary-structure algorithms. However, this strand, through its hydrogen bonds, contributes an important element of cohesion between the two ($\alpha\beta$) modules and should therefore be part of the topology of the protein.

A superposition of the C^{α} atoms of all four asparaginase models highlights several chain fragments that are less consistent. As a rule, these fragments are located at the surface, or even protrude from the protein surface, and therefore are naturally more flexible, have higher *B* factors and are often defined in inferior electron density. Several of these differences can be described as a concerted shift of a similar structural element. In two areas, however, the main chain has a different fold. These areas correspond to loops that are also flexible among the three PvAspG1 structures: residues Gly13–Gln23 in subunit α and Arg283–Lys288 in subunit β (Fig. 6). The conformation of these loops is probably connected with substrate specificity and/or potassium dependence, as discussed below.

The variable loop at the carboxyl end of the α subunit, which is freed during protein maturation, has a highly variable sequence and is usually totally disordered in the crystal structures of mature plant-type L-asparaginases. Interestingly, two of the four α subunits present in the asymmetric unit of the LlA structure (Michalska *et al.*, 2006) could be modelled with several more residues at the C-terminus than in the PvAspG1 structures. The α-subunit tail of LlA covers the active-site area but does not interact with any of the residues that form the active site, the metal-binding loops or the catalytic switch in PvAspG1. However, the LlA structure shows that the side chain of Tyr165 at the C-terminal tail of subunit α forms a weak OH$\cdots$O hydrogen bond with Gly10, which (as Gly9) is important for hASNase3 maturation.

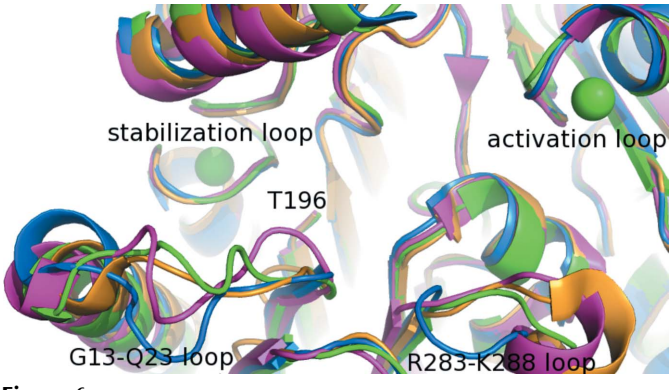

Figure 6
Some flexible regions of plant-type L-asparaginases: loops comprising residues Gly13–Gln23 in subunit α and Arg283–Lys288 in subunit β. Cartoon representation of superposed C^{α} traces of PvAspG1–K (green), LlA (blue), EcAIII (pink) and hASNase3 (orange). The metal cations (green spheres) in the stabilization and activation loops are from the PvAspG1–K structure. Labels and numbering are according to the PvAspG1–K structure: Gly13–Gln23 from subunit α (chain *C*) and Arg283–Lys288 from subunit β (chain *D*).

The metal-binding loops of LlA, EcAIII and hASNase3, corresponding to the stabilization loop of PvAspG1, are all occupied by sodium ions. Because those loops coordinate the central ion exclusively through main-chain carbonyl groups, their amino-acid sequence influences only the fitting of the loop inside the rest of the structure in this area. Thus, despite the differences in the stabilization-loop sequences among plant-type L-asparaginases (Supplementary Table S2), and the different metal cations occupying this loop in the PvAspG1 structures, the general shape of this loop is preserved. The trace of the main chain, as well as the coordination geometry, are similar in all the discussed structures. Moreover, the Asn65 residue of PvAspG1, whose main-chain C=O group is important for the stabilizing function, has its conformation and position in space exactly preserved in all cases. In conclusion, the stabilization loop is constructed in such a way that it can utilize different metal cations to support its stabilizing function.

The residues that create the activation loops in the K-dependent PvAspG1 (Val111–Ser118) also form loops in the K-independent enzymes, with the main-chain C=O groups directed towards the loop centre. The occupancy of these loops is surprisingly variable. In most cases, a water molecule has been modelled inside the loop. In the LlA structure (Michalska *et al.*, 2006) these loops are occupied by well modelled water molecules (two loops) or remain empty (two loops). As a summary of all of the EcAIII structures available in the PDB (six models, *i.e.* 12 α subunits), there are water molecules (eight loops), a Tris molecule (one loop), a calcium ion (one loop) and two Na^{+} ions (in the two loops of PDB entry 3c17). In the latter case, Na^{+} ions are also present at nine other places in the crystal structure, including both active sites, both stabilization loops and five additional sites at the surface of the protein. Such a situation is possible because the crystallization buffer contained a very high (4.3 *M*) NaCl concentration. In the hASNase3 structures (PDB entries 4gdt, 4gdu, 4gdv, 4gdw, 4hlo and 4hlp) the activation loops are empty (two loops), occupied by water molecules (six loops) or occupied by a glycine molecule (four loops) used during crystal preparation. However, it seems that such a diversified landscape of the activation-loop occupancies is only an artifact of crystallization and that only the loops observed in the PvAspG1 structures have evolved for specific alkali-metal coordination, as in all cases, regardless of the crystallization conditions, the loops are occupied by such ions.

In all three K-independent protein structures the conformation of the activation loop resembles that in PvAspG1, or more specifically in PvAspG1–K, where the catalytic switch is

turned ON. The sequences of the activation loop are quite variable among L-asparaginases, but one of the catalytic switch residues, His117, is conserved in all cases (Supplementary Table S2). It seems that the specific affinity for alkali-metal cations and the ability to switch the catalytic mechanism may be associated with the presence of Ser118 in the activation loop. This residue is responsible for the proper positioning of water molecules coordinated by the metal ion and is also tuned with the conformational changes of Glu250, another catalytic switch residue. Ser in this position is not present in potassium-independent L-asparaginases, but is strictly conserved in the potassium-dependent enzymes.

A comparison of the active site of PvAspG1–K with the same area of the crystal structures of mature K-independent enzymes, LlA, EcAIII and hASNase3, shows a high degree of conservation in terms of both sequence and structure, regardless of the presence of a product/substrate molecule. Moreover, the L-aspartate occupying the two active sites of EcAIII (PDB entry 2zal) and hASNase3 (PDB entry 4gdw) is in exactly the same orientation and conformation as the single L-Asp molecule in the PvAspG1–K structure. The active sites of PvAspG1–Na and PvAspG1–K/Na are different because of the reorientation of the Arg224 side chain in the catalytic switch.

The amino-acid residues that form the catalytic switch in PvAspG1 (His117, Arg224 and Glu250) are also conserved in LlA, EcAIII and hASNase3 (Supplementary Table S2). Moreover, in all (K-independent) L-asparaginase structures known to date the conformation of the catalytic switch triad closely resembles the situation in the *AB* heterodimer of the PvAspG1–K structure, *i.e.* it corresponds to the activated state with a potassium ion in the activation loop and L-aspartate in the active site. We can therefore conclude that the K-independent enzymes such as LlA, EcAIII or hASnase3 are permanently in the ON state, even without potassium ions.

4.3. The problem of autocatalytic maturation of PvAspG1

To adopt the mature form, plant-type L-asparaginases undergo spontaneous breakdown into a larger (α) and smaller (β) subunits. The rate of this process is variable; for instance, self-cleavage of EcAIII takes place in a matter of hours, while that of LlA takes place in a matter of days. The mechanism of the autocatalytic maturation of plant-type L-asparaginases was first proposed by Michalska, Hernández-Santoya *et al.* (2008) on the basis of the crystal structure of an active-site mutant (T179A) of EcAIII. This mechanism indicates several elements that are necessary for the maturation process: the catalytic Thr179 residue (which acts as the nucleophile in both reactions), a general base Thr230, and Asn67 (from the stabilization loop), the side chain of which is part of the oxyanion hole for the O atom of the scissile peptide. An alternative mechanism controls the maturation of recombinant hASNase3, which undergoes self-cleavage at a very slow rate, selectively accelerated by the free amino acid glycine (Nomme *et al.*, 2012; Su *et al.*, 2013). The glycine cofactor is positioned in close proximity to the catalytic Thr168 residue and is believed to act as a general base initiating the cleavage reaction. To complicate the situation even further, the autocleavage site in different immature plant-type L-asparaginases (PDB entries 3c17, 2zak, 4gdu and 4hlo) shows variable conformation, leading to different interactions with the Thr nucleophile.

Since the structure of immature PvAspG1 is not known, it is not possible to speculate about the specific maturation mechanism. However, some observations indicate that PvAspG1 is most likely to mature according to the mechanism proposed for EcAIII. First of all, recombinant PvAspG1 is cleaved very quickly, in a matter of minutes or seconds, probably immediately after folding inside the host cell, because the mature subunits are already present in the protein-isolation step (visible on SDS–PAGE). Secondly, at variance with hASNase3, free glycine is not necessary for PvAspG1 maturation.

4.4. The mechanism of the reaction catalyzed by PvAspG1

Plant-type L-asparaginases are known to catalyze two hydrolysis reactions at the side chain of L-asparagine. The L-asparaginase activity releases ammonia from L-asparagine, while the isoaspartyl aminopeptidase activity separates two amino acids linked by a β-amide bond at the asparagine side chain. The general mechanism of the reaction catalyzed by mature plant-type L-asparaginase is similar to that of classic serine proteases (Dodson & Wlodawer, 1998), although the enzyme does not use a catalytic triad (Michalska & Jaskolski, 2006). The proposed mechanism has been reviewed in detail by Nomme *et al.* (2012). The most important feature of this proposal is that, in keeping with the general mechanism of Ntn-hydrolases, the nucleophilic group of the catalytic threonine is believed to be activated by the free α-amino group of the same residue, functioning as a general base. This view is not without doubt, mainly because stereochemical considerations do not favour a strained intramolecular $O-H\cdots NH_2$ hydrogen bond. Moreover, an N-terminal $-NH_2$ group is a rather weak hydrogen abstractor from a hydroxyl group, and is easily protonated to the $-NH_3^+$ ammonium form, which cannot act as an abstractor (Michalska & Jaskolski, 2006).

A key role in facilitating proton abstraction from the nucleophile may be played by the contact between the catalytic threonine and an asparagine residue located in the stabilization loop (Michalska *et al.*, 2005). In all present models of PvAspG1, there is a hydrogen-bond interaction between the free α-amino group of the catalytic Thr196 and the main-chain carbonyl group of Asn65. An identical interaction is present in LlA and EcAIII. It is also very likely that this contact provides the correct orientation of the catalytic threonine. Alternatively, it was proposed for hASNase3 that the amino group of the catalytic threonine may directly activate its hydroxyl group and that nearby water molecules, held in position by the side chain of the stabilization-loop asparagine, could help to shuttle the proton (Nomme *et al.*, 2012). However, such a situation with only indirect interactions between the threonine and asparagine residues, mediated by

three water molecules, is rather rare even among hASNase3 models. In the PvAspG1 models, the catalytic Thr196 usually has contacts with two water molecules (rarely with one or no water molecules), but never breaks its contact with the main-chain carbonyl of Asn65. Thus, despite the growing evidence about the interactions in the L-asparaginase active site, the overall picture seems to be rather complicated. It would be very helpful to visualize the active site with a substrate molecule (and not only with a reaction product) in order to analyze the movements of the key residues and water molecules.

4.5. Substrate specificity of PvAspG1

Our biochemical studies have confirmed the potassium dependence of the L-asparaginase activity of the enzyme (Table 2), but the substrate-specificity profile has not been studied. However, since PvAspG1 and LjNSE1 have 96% sequence similarity, it is highly probable that the two enzymes share the same substrate preferences. Moreover, one of the active sites in the PvAspG1–K structure is occupied by L-aspartate, which is a product molecule common to several possible reactions. This allows us to speculate about the theoretically possible substrates based on comparisons with similar Ntn-amidohydrolases.

Biochemical studies of LlA and EcAIII showed that L-asparagine was not hydrolyzed if it had a modification at either the α-carboxyl or the α-amino group (Borek *et al.*, 2004). These observations are also consistent with the PvAspG1–K structure, as both of the mentioned groups are critically involved in docking the product molecule in the active site (Fig. 2). The α-amino group interacts with residues Asp227 and Gly247, and the α-carboxyl group with Arg224 and Gly249. Moreover, as described above, the fork of salt-bridge/hydrogen bonds created at the side chain of Arg224 efficiently immobilizes the ligand, docking it precisely in the active site. The length of the arginine side chain can be considered to be a measuring rod that places the small substrate molecule (unsuitable for extensive recognition by specificity pockets of the protein) in the precisely designated point in the active site, so that the β-amide group is appropriately poised for attack by the Thr196 nucleophile. The distance between the tip of the Arg224 side chain and the catalytic Thr196 determines the length of the substrate, or the exact site where the hydrolysis reaction takes place (Michalska & Jaskolski, 2006). Thus, any L-aspartate-derived small molecules, such as L-asparagine or related β-peptides (*e.g.* β-Asp-Leu) are potential substrates, but the side chain of L-glutamine is too long to be hydrolyzed by LlA or EcAIII (Borek *et al.*, 2004) and probably also by PvAspG1–K.

The same PvAspG1 protein but with Na^+ in the metal-binding loops (PvAspG1–Na) no longer fits the above scenario. The Arg224 element of the catalytic switch flips its side chain by ~180°, which is sufficient to destroy the stability of the docking scaffold. The rest of the active-site cavity of PvAspG1–Na does not change very much, which explains why this metal-controlled conformational transition only reduces the catalytic efficiency, rather than deactivating the enzyme completely. In Tas1 (Khan *et al.*, 2005), where the activation loop does not exist at all and where the catalytic switch histidine is replaced by a much smaller proline, the side chain of the arginine anchor can 'swing away' from the active site by about 60° (Fig. 7). Such a different orientation of the arginine element allows the anchoring of a larger substrate group, specifically the β-carboxylate of the -Xxx-(α-Asp)-Gly-Xxx- motif of the MML (mixed-lineage leukaemia) protein substrate. It is therefore conceivable that a metal-cation exchange in the PvAspG1 enzyme might not only regulate the efficiency of L-Asn hydrolysis, but could also change the substrate preference. Further studies, both structural and biochemical, are needed to confirm this speculation.

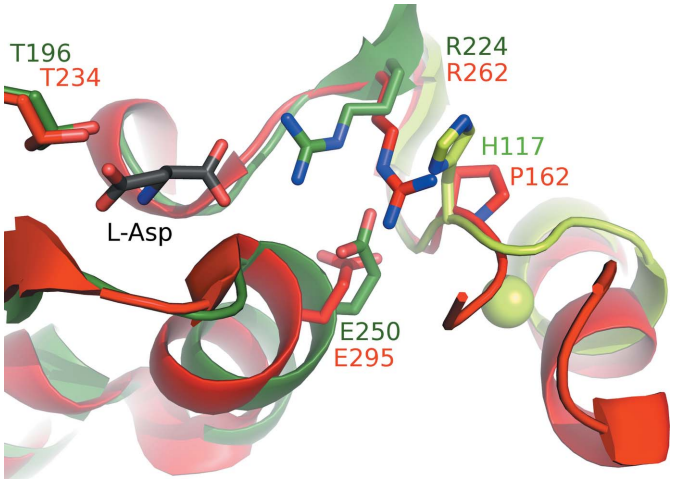

Figure 7
Comparison of the active-site areas of PvAspG1–K and Tas1. Cartoon representation of C^{α} superposition of PvAspG1–K (chain *B*, dark green; chain *C*, light green) and Tas1 (red) with labels coloured to match the models. The K^+ ion in the activation loop (light green sphere) and L-Asp (grey sticks) are elements from the PvAspG1–K structure.

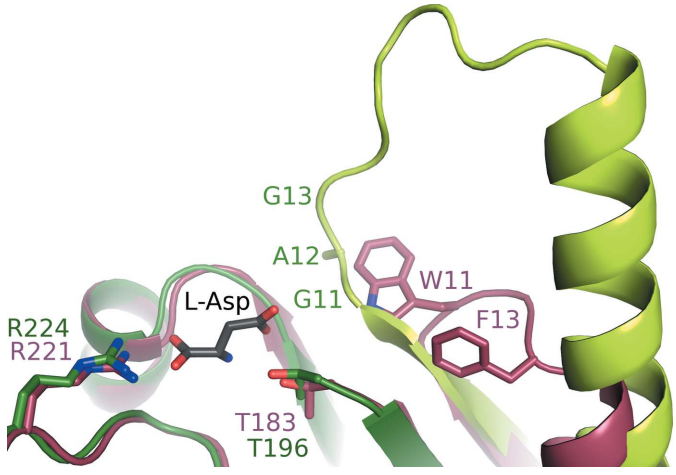

Figure 8
Comparison of the active-site areas of PvAspG1–K and AGA. Cartoon representation of C^{α} superposition of PvAspG1–K (chain *B*, dark green; chain *A*, light green) and AGA (raspberry) with labels coloured to match the models. L-Asp (grey sticks) is an element from the PvAspG1–K structure.

In aspartylglucosaminidase (AGA), another relative of plant-type Ntn-hydrolases, an extension of the active-site cavity is formed by a small loop with two aromatic residues, Trp11 and Phe13, which bind the sugar moiety of the substrate (Oinonen *et al.*, 1995; Guo *et al.*, 1998; Xuan *et al.*, 1998). Glycosylated L-asparagine is far too large to fit inside the PvAspG1 active site. This area in PvAspG1, as well as in LlA (Michalska *et al.*, 2006) and EcAIII (Michalska *et al.*, 2005), is built by a long loop starting with a stretch of small residues in the GAG motif (Gly11-Ala12-Gly13; Supplementary Table S2; Fig. 8). The GAG motif is expected to interact with the residue in the β-position of β-Asp-peptide substrates. An analogous GAG motif in the Tas1 protease is shifted out of the ligand-binding position, allowing the accommodation of a longer substrate. Interestingly, the peptide group of Ala48 in Tas1 assumes different orientations in the two α subunits with a 180° flip, analogously to the corresponding carbonyl groups of Gly9 in mature and immature hASNase3 (Nomme *et al.*, 2012; Su *et al.*, 2013). The long loop comprised of residues Gly13–Gln23 (PvAspG1 numbering) is among the most variable elements of plant-type L-asparaginases in terms of both sequence and structure. For this reason, it can be considered to be an important element determining substrate specificity.

The variable loop at the C-terminus of subunit α has also been implicated as a specificity determinant of plant-type L-asparaginases (Gabriel *et al.*, 2012). A reciprocal exchange of segments of the variable loop between similar K-dependent and K-independent enzymes (both from *A. thaliana*) did influence the catalytic activity, confirming the importance of this region (Gabriel *et al.*, 2012). In the LlA structure (Michalska *et al.*, 2006), where a longer stretch at the C-terminus of subunit α could be traced in the electron-density maps, the tail is blocking the entrance to the active-site cavity. Moreover, molecular-dynamics simulations suggest that monovalent cation binding to LjNSE1 might induce a conformational change at the C-terminal end of the α subunit, favouring substrate binding (Credali *et al.*, 2011). In conclusion, the C-terminal end of the α subunit may contain structural determinants that influence, directly or indirectly, the substrate preferences of plant-type L-asparaginases. However, it is not possible to verify such speculations structurally, as the models of PvAspG1 (as well as of EcAIII and hASNase3) are incomplete in this area.

4.6. Critical review of earlier noncrystallographic studies of K-dependent asparaginases

Based on homology modelling and molecular-dynamics studies, complemented with site-directed mutagenesis, Credali *et al.* (2011) identified a region within the K-dependent L-asparaginase from *L. japonicus* (LjNSE1) that purportedly exhibited potential for K^+ binding. The study indicated Glu248, Asp285 and Glu286 as the key residues for K^+ coordination and thus for stimulation of the L-asparaginase activity. The sequences of PvAspG1 and LjNSE1 are almost identical (91%) and the above residues are fully conserved as to their type and even their numbering; therefore, a high degree of similarity between their structures is expected. The equivalent region in PvAspG1 is created by a loop of six residues (Arg283–Lys288) located in subunit β between helix βH3 and strand βS6. A superposition of the C^α traces of PvAspG1, LlA, EcAIII and hASNase3 shows a considerable variation of the loop conformation (Fig. 6), suggesting its flexibility and potential role in enzyme activity.

A comparison of the six copies of this region in the three PvAspG1 structures presented here revealed that the surface-exposed side chains of helix βH3 are quite flexible, whereas in strand βS6 they are firmly fixed. The loop linking βH3 and βS6 has a variable and generally poor electron density, although the main-chain trace is unambiguous. The best defined loop, of PvAspG1–K chain *B*, does not have electron density for six atoms (in total) located in two side chains (Glu286, Lys288). Since it is not possible to compare the entire Arg283–Lys288 loops in PvAspG1–K, PvAspG1–Na and PvAspG1–K/Na in full detail, the most interesting residues, Glu248, Asp285 and Glu286, will be analyzed on the basis of their models derived from good electron density only.

Asp285 and Glu286 are located inside the Arg283–Lys288 loop. The side chain of Asp285 is fully visible in both subunits of the PvAspG1–K structure, interacting with the side chains of Arg254 and Arg90 (Fig. 9). The distance to the nearest K^+ ion (in the activation loop) is ∼16 Å. The side chain of Glu286 is well defined only in chain *D* of PvAspG1–Na, where it interacts only with the side chain of Arg254 and is ∼13 Å away from the Na^+ cation in the activation loop. Asp285 and Glu286 are too distant to influence the active site, the catalytic switch or the metal-binding loops. It is not possible to compare these residues with the corresponding residues in LlA, EcAIII and

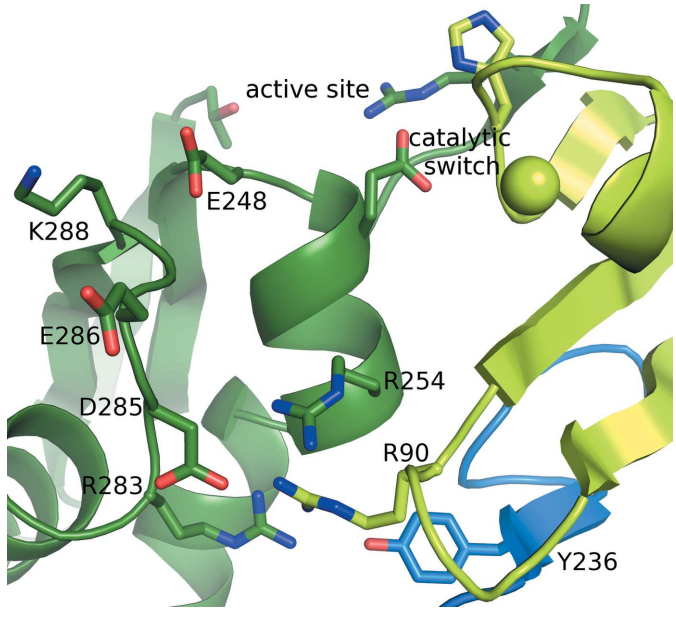

Figure 9
The molecular environment of Glu248, Asp285 and Glu286. These residues were postulated by Credali *et al.* (2011) to be the potassium binding site. Cartoon representation of PvAspG1–K (chain *A*, light green; chain *D*, dark green; chain *B*, blue) with K^+ in the activation loop (light green sphere) with some key residues labelled.

hASNase3 because the main chain traces very different shapes in these models.

Glu248 is located in a very important area of subunit β between strand βS5 (harbouring Thr246 and Gly247 engaged in L-Asp binding) and helix βH1 (harbouring Gly249, which is also engaged in L-Asp binding, and the Glu250 element of the catalytic switch). All six copies of Glu248 have the same conformation. The main-chain C=O group participates in the hydrogen-bond pattern of helix βH1, while the side chain interacts with the main chain of the adjacent Lys288 from the Arg283–Lys288 loop (Fig. 9). Despite its prominent location, Glu248 does not interact directly with the active site, the metal-binding loops or any of the coordinated metal ions themselves, with the average distance to the metal ion in the activation loop being ~13 Å. At the corresponding location in the LlA structure, the side chain of Lys245 does not form any hydrogen bonds at all; in EcAIII the side chain of Thr232 interacts with the adjacent loop analogously to Glu248 in PvAspG1, and in hASNase3 the side chain of His221 is hydrogen-bonded to residue Glu223 (corresponding to the catalytic switch element Glu250 in PvAspG1) and to Ser224.

Credali *et al.* (2011) complemented their analyses with side-directed mutagenesis and biochemical tests. Replacement of Glu248-Asp285-Glu286 with Lys248-Pro285-Lys286 (as in the sequence of the *L. japonicus* K-independent L-asparaginase LjNSE2 with preferred β-aspartyl-peptidase activity) resulted in a lowering of the enzymatic activity with L-asparagine as a substrate independently of the presence or absence of potassium. In the PvAspG1 structure, similar mutations of Asp285 and Glu286 would lead to increased destabilization of the Arg283–Lys288 loop because of abrogation of the interactions with Arg254 and Arg90. In the case of Glu248, it is difficult to explain why this residue was so crucial in the study of Credali *et al.* (2011).

Notwithstanding all of the above reservations, the crystal structures of PvAspG1 clearly demonstrate that none of the residues proposed by Credali *et al.* (2011) (Glu248, Asp285 and Glu286) has any role in metal coordination or otherwise influences the active site, the catalytic switch mechanism or the metal-binding loops (Fig. 9). Although these residues are located in the vicinity of a catalytically important area, their linear spatial disposition precludes the creation of a stereochemically viable metal-binding site. Besides, if (any of) these residues were involved in K^+ coordination, this area would have been much more stable, likely with excellent electron density. It is more likely that Asp285 and Glu286 are responsible for substrate preference rather than potassium dependence, and influence the enzyme activity in this way. Moreover, we note that besides Asp285 and Glu286, the Arg283–Lys288 loop contains another even more crucial residue, Arg283. Among the three PvAspG1 models, four out of the six Arg283 side chains have very good electron density, illustrating that this residue connects three of the four protein chains; *e.g.* Arg283*D* (from chain *D*) interacts with Gly255*D*, Thr256*D*, Arg90*A* and Tyr236*B*. Thus, the location of Asp285 and Glu286 near the $\alpha\beta$–$\alpha\beta$ interface between the two heterodimers is very suggestive of the importance of these residues for quaternary-structure stabilization. On the other hand, if this were their main role in the structure of PvAspG1, these residues, and very likely the entire Arg283–Lys288 loop, would be expected to be much more rigid than in the present PvAspG1 models. In conclusion, it is likely that the entire Arg283–Lys288 loop, rather than the individual residues Glu248, Asp285 and Glu286, is important for enzyme activity. These and other exciting aspects of PvAspG1 structure and function require further investigation.

4.7. Conclusions regarding potassium (in)dependence

The three crystal structures of the potassium-dependent plant-type L-asparaginase PvAspG1 demonstrate that the enzyme is capable of coordinating two different alkali-metal cations in two entirely different binding sites. The first binding site, located in the stabilization loop (residues Leu58–Arg68), so named because of its role in stabilizing the geometry of the catalytic apparatus, had previously been identified in plant-type L-asparaginases as the 'sodium loop'. This loop, or strictly speaking a particular asparagine residue in its sequence, may also be directly or indirectly responsible for the reaction mechanism, as it interacts with the nucleophilic residue in the active site. Surprisingly, potassium/sodium exchange at this site does not appear to influence the enzyme active site. However, it is possible that other ions, *e.g.* Li^+ or Rb^+, could interrupt the stabilization-loop conformation and function.

The second metal-binding site, termed the activation loop (residues Val111–Ser118), is a novel feature found only in this K-dependent enzyme, and absent in the previous structures of K-independent plant-type L-asparaginases. The metal cation coordinated at this site affects the enzyme activity through a mechanism that is based on a conformational change of the catalytic switch comprised of residues His117, Arg224 and Glu250. The switch has two states: ON when K^+ is bound and OFF when Na^+ is bound. The two conformations respectively allow and prevent anchoring of the L-Asp product in the active site. The remaining elements of the active-site cavity (*i.e.* the catalytic Thr, the oxyanion hole *etc.*) have a fairly conserved conformation that is insensitive to the type of metal cation present in the activation loop. This may explain why switching the activation loop to the OFF configuration does not deactivate the enzyme completely, but leaves a residual asparaginase activity even in the absence of potassium cations. On the other hand, the structure of Tas1 suggests that exchange of the metal cation in the activation loop might (in addition to tuning the asparaginase activity) modify the substrate specificity as well. Additional biochemical studies are needed to verify this idea.

Based on the PvAspG1 structure, we are unable to explain why the highly similar (in terms of sequence) LjNSE1 L-asparaginase is reportedly incapable of hydrolyzing β-peptides. This is particularly puzzling as this substrate would be expected to be identically anchored in the active site and as the GAG motif, which is responsible for substrate recognition, is present (and rather conserved) in both the K-dependent and the K-independent enzymes.

A comparison of the two $\alpha\beta$ heterodimers in the PvAspG1–K structure shows that both have K^+ ions bound in the activation loops and the catalytic switch residues in the ON state, even though only one active site is occupied by an L-Asp ligand. We thus conclude that the state of active-site occupation has no influence on the behaviour of the catalytic switch residues and that only the coordinated metal cations are responsible for triggering this mechanism.

Our analysis of PvAspG1 explains the significance of its quaternary structure, *i.e.* why this potassium-dependent enzyme forms an obligatory $(\alpha\beta)_2$ dimer of heterodimers. Since the active site of one heterodimer (*e.g. AB*) is controlled by the activation loop from the other heterodimer (*CD*) through the catalytic switch residues Arg224 and Glu250 (from chain *B*) and His117 (from chain *C*), this mechanism can only work within a dimer of heterodimers.

Finally, we postulate that Ser118, the last residue of the activation loop, is of key importance for the potassium dependence of PvAspG1. Ser118 forms hydrogen bonds to water molecules in the coordination sphere of the metal ion in the activation loop and also mediates the conformational changes of Glu250 in the catalytic switch triad. However, this proposition must be confirmed, for example by site-directed mutation experiments.

The K^+ concentration is usually two orders of magnitude higher than the Na^+ concentration in plant cells (Chérel *et al.*, 2014). Enzymes activated by monovalent cations are stimulated by K^+ when they are intracellular and by Na^+ when they are extracellular (Page & Di Cera, 2006). This indicates that the Na/K switch is unlikely to serve regulatory purposes. Nevertheless, its occurrence in the K-dependent asparaginase is very intriguing. Since soil salinity arising from irrigation is a major problem in global agriculture, it is reasonable to assume that as the intracellular Na^+ concentration rises the K-dependent asparaginase activity will be affected.

This work was supported in part by a Discovery Grant from the Natural Sciences and Engineering Research Council of Canada (NSERC) to FM.

References

Adams, P. D. *et al.* (2010). *Acta Cryst.* D**66**, 213–221.
Allen, F. H. (2002). *Acta Cryst.* B**58**, 380–388.
Altschul, S. F., Madden, T. L., Schäffer, A. A., Zhang, J., Zhang, Z., Miller, W. & Lipman, D. J. (1997). *Nucleic Acids Res.* **25**, 3389–3402.
Berman, H. M., Westbrook, J., Feng, Z., Gilliland, G., Bhat, T. N., Weissig, H., Shindyalov, I. N. & Bourne, P. E. (2000). *Nucleic Acids Res.* **28**, 235–242.
Borek, D. (2001). PhD thesis. A. Mickiewicz University, Poznan, Poland.
Borek, D. & Jaskólski, M. (2000). *Acta Cryst.* D**56**, 1505–1507.
Borek, D. & Jaskólski, M. (2001). *Acta Biochim. Pol.* **48**, 893–902.
Borek, D., Michalska, K., Brzezinski, K., Kisiel, A., Podkowinski, J., Bonthron, D. T., Krowarsch, D., Otlewski, J. & Jaskolski, M. (2004). *Eur. J. Biochem.* **271**, 3215–3226.
Brannigan, J. A., Dodson, G., Duggleby, H. J., Moody, P. C., Smith, J. L., Tomchick, D. R. & Murzin, A. G. (1995). *Nature (London)*, **378**, 416–419.
Brese, N. E. & O'Keeffe, M. (1991). *Acta Cryst.* B**47**, 192–197.
Brown, I. D. (2009). *Chem. Rev.* **109**, 6858–6919.
Bruneau, L., Chapman, R. & Marsolais, F. (2006). *Planta*, **224**, 668–679.
Cantor, J. R., Stone, E. M., Chantranupong, L. & Georgiou, G. (2009). *Biochemistry*, **48**, 11026–11031.
Chérel, I., Lefoulon, C., Boeglin, M. & Sentenac, H. (2014). *J. Exp. Bot.* **65**, 833–848.
Credali, A., Díaz-Quintana, A., García-Calderón, M., De la Rosa, M. A., Márquez, A. J. & Vega, J. M. (2011). *Planta*, **234**, 109–122.
DeLano, W. L. (2002). *PyMOL*. http://www.pymol.org.
Dodson, G. & Wlodawer, A. (1998). *Trends Biochem. Sci.* **23**, 347–352.
Emsley, P. & Cowtan, K. (2004). *Acta Cryst.* D**60**, 2126–2132.
Gabriel, M., Telmer, P. G. & Marsolais, F. (2012). *Planta*, **235**, 1013–1022.
Guo, H. C., Xu, Q., Buckley, D. & Guan, C. (1998). *J. Biol. Chem.* **273**, 20205–20212.
Harding, M. M. (2006). *Acta Cryst.* D**62**, 678–682.
Harding, M. M., Nowicki, M. W. & Walkinshaw, M. D. (2010). *Crystallogr. Rev.* **16**, 247–302.
Ho, P. P. K., Milikin, E. B., Bobbitt, J. L., Grinnan, E. L., Burck, P. J., Frank, B. H., Boeck, L. D. & Squires, R. W. (1970). *J. Biol. Chem.* **245**, 3708–3715.
Kabsch, W. (2010). *Acta Cryst.* D**66**, 125–132.
Karamitros, C. S. & Konrad, M. (2014). *Protein Expr. Purif.* **93**, 1–10.
Khan, J. A., Dunn, B. M. & Tong, L. (2005). *Structure*, **13**, 1443–1452.
Krissinel, E. & Henrick, K. (2004). *Acta Cryst.* D**60**, 2256–2268.
Kuppuraj, G., Dudev, M. & Lim, C. (2009). *J. Phys. Chem. B*, **113**, 2952–2960.
Langer, G., Cohen, S. X., Lamzin, V. S. & Perrakis, A. (2008). *Nature Protoc.* **3**, 1171–1179.
Li, W., Cantor, J. R., Yogesha, S. D., Yang, S., Chantranupong, L., Liu, J. Q., Angello, G., Georgiou, G., Stone, E. M. & Zhang, Y. (2012). *ACS Chem. Biol.* **7**, 1840–1847.
McCoy, A. J., Grosse-Kunstleve, R. W., Adams, P. D., Winn, M. D., Storoni, L. C. & Read, R. J. (2007). *J. Appl. Cryst.* **40**, 658–674.
Michalska, K., Borek, D., Hernández-Santoyo, A. & Jaskolski, M. (2008). *Acta Cryst.* D**64**, 309–320.
Michalska, K., Brzezinski, K. & Jaskolski, M. (2005). *J. Biol. Chem.* **280**, 28484–28491.
Michalska, K., Bujacz, G. & Jaskolski, M. (2006). *J. Mol. Biol.* **360**, 105–116.
Michalska, K., Hernández-Santoyo, A. & Jaskolski, M. (2008). *J. Biol. Chem.* **283**, 13388–13397.
Michalska, K. & Jaskolski, M. (2006). *Acta Biochim. Pol.* **53**, 627–640.
Murshudov, G. N., Skubák, P., Lebedev, A. A., Pannu, N. S., Steiner, R. A., Nicholls, R. A., Winn, M. D., Long, F. & Vagin, A. A. (2011). *Acta Cryst.* D**67**, 355–367.
Nomme, J., Su, Y., Konrad, M. & Lavie, A. (2012). *Biochemistry*, **51**, 6816–6826.
Oinonen, C., Tikkanen, R., Rouvinen, J. & Peltonen, L. (1995). *Nature Struct. Biol.* **2**, 1102–1108.
Page, M. J. & Di Cera, E. (2006). *Physiol. Rev.* **86**, 1049–1092.
Painter, J. & Merritt, E. A. (2006*a*). *Acta Cryst.* D**62**, 439–450.
Painter, J. & Merritt, E. A. (2006*b*). *J. Appl. Cryst.* **39**, 109–111.
Park, S. J. & Rupert, T. (2000). *Can. J. Plant Sci.* **80**, 341–342.
Prahl, A., Pazgier, M., Hejazi, M., Lockau, W. & Lubkowski, J. (2004). *Acta Cryst.* D**60**, 1173–1176.
Satow, Y., Cohen, G. H., Padlan, E. A. & Davies, D. R. (1986). *J. Mol. Biol.* **190**, 593–604.
Sheldrick, G. M. (2008). *Acta Cryst.* A**64**, 112–122.
Sodek, L., Lea, P. J. & Miflin, B. J. (1980). *Plant Physiol.* **65**, 22–26.
Su, Y., Karamitros, C. S., Nomme, J., McSorley, T., Konrad, M. & Lavie, A. (2013). *Chem. Biol.* **20**, 533–540.
Swain, A. L., Jaskólski, M., Housset, D., Rao, J. K. M. & Wlodawer, A. (1993). *Proc. Natl Acad. Sci. USA*, **90**, 1474–1478.
Thorn, A. & Sheldrick, G. M. (2011). *J. Appl. Cryst.* **44**, 1285–1287.
Verma, N., Kumar, K., Kaur, G. & Anand, S. (2007). *Crit. Rev. Biotechnol.* **27**, 45–62.

Winn, M. D. *et al.* (2011). *Acta Cryst.* D**67**, 235–242.
Xuan, J., Tarentino, A. L., Grimwood, B. G., Plummer, T. H. Jr, Cui, T., Guan, C. & Van Roey, P. (1998). *Protein Sci.* **7**, 774–781.
Zheng, H., Chordia, M. D., Cooper, D. R., Chruszcz, M., Müller, P., Sheldrick, G. M. & Minor, W. (2014). *Nature Protoc.* **9**, 156–170.
Zheng, H., Chruszcz, M., Lasota, P., Lebioda, L. & Minor, W. (2008). *J. Inorg. Biochem.* **102**, 1765–1776.